Analysis of optical coatings and thin films

M.Tech. Thesis

By

SHRUTI PANKAJ SHARMA

DEPARTMENT OF MECHANICAL ENGINEERING

INDIAN INSTITUTE OF TECHNOLOGY INDORE

JUNE 2025

Analysis of optical coatings and thin films

A THESIS

Submitted in partial fulfillment of the
requirements for the award of the degree
of
Master of Technology

by
SHRUTI PANKAJ SHARMA

DEPARTMENT OF MECHANICAL ENGINEERING
INDIAN INSTITUTE OF TECHNOLOGY INDORE
JUNE 2025

INDIAN INSTITUTE OF TECHNOLOGY INDORE

CANDIDATE'S DECLARATION

I hereby certify that the work which is being presented in the thesis entitled **Analysis of optical coatings and thin films** in the partial fulfillment of the requirements for the award of the degree of **MASTER OF TECHNOLOGY** and submitted in the **DEPARTMENT OF MECHANICAL ENGINEERING, Indian Institute of Technology Indore**, is an authentic record of my own work carried out during the time period from July, 2023 to June, 2025 under the supervision of Prof. Krushna R. Mavani, Department of Physics, Indian Institute of Technology Indore and Dr. Suparna Pal, Optical Coatings Laboratory, High Energy Lasers and Optics Section, Raja Ramanna Centre for Advanced Technology,(Government of India, Department of Atomic Energy), Indore.

The matter presented in this thesis has not been submitted by me for the award of any other degree of this or any other institute.

11/07/2025

Signature of the student with date

Shruti Pankaj Sharma

This is to certify that the above statement made by the candidate is correct to the best of my/our knowledge.

11.07.2025

Signature of Supervisor of
M.Tech thesis #1 (With Date)

Prof. Krushna R. Mavani

Suparna Pal 23.05.2025

Signature of Supervisor of
M.Tech thesis #2 (With Date)

Dr. Suparna Pal

Shruti Pankaj Sharma has successfully given his/her M.Tech. Oral Examination held on **9th May, 2025**

Signature(s) of Supervisor(s) of M.Tech. thesis

Date: 11.07.2025

Suparna Pal 23.05.2025

Convener, DPGC

Date: 15-07-2025

ACKNOWLEDGEMENTS

I would like to express my sincere gratitude to my guide, ***Professor Krushna R. Mavani****, Department of Physics, for her undivided attention, patience and guidance towards this project. Her insights and remarks played a pivotal role in the execution of this work.*

My profound thanks and gratitude to ***Dr. Suparna Pal****, Scientific Officer G, (OTFCS), HELOS, RRCAT Indore for her encouragement and patience. She is not only a recognized scientist but also an incredible teacher which was reflected through her guidance, support and enthusiasm towards this project.*

My heartfelt gratitude towards ***Dr. Rajiv Kamparath*** *and* ***Dr. Neha Sharma*** *who helped me innumerous times and also took out the time to make sure I understood the concepts behind the experimental part of the project.*

I sincerely thank ***Shri N.S. Banerjee****, HOD, High Energy Lasers and Optics Section for helping me every step of the way through this project. His kind support and encouragement is something I am extremely grateful for.*

Heartiest thanks to ***Mr. Lokendra Chandravanshi*** *for his guidance and help.*

My sincere thanks to ***Mr. Manish Kumar*** *for his time and efforts in helping through the project. I am grateful for his patience and criticism.*

A very sincere thanks to ***Dr. Rahul Shukla****,* ***Dr. Shilpam Sharma****,* ***Dr. Neha Sharma and Mr. Varun Sharma****, for helping me out through the electrode fabrication process. I had found myself stuck if not for their help and guidance. They went out of their way to help me out for which I would be eternally grateful.*

I would like to express my heartfelt appreciation to ***Dr. Rudraksh Nagar****.*

Lastly, the most important thanks to ***Mr. Pankaj Sharma****,* ***Mrs. Kusum Sharma****,* ***Ms. Krati Sharma and Vanshika*** *for being the most supportive and loving family anyone could ask for. Deepest regards for their love, care and inspiration.*

DEDICATION

For (Late) Dr. Murli Manohar Sharma, beloved grandfather and teacher.

Abstract

We report the fabrication of interdigitated electrodes on Ga doped ZnO thin film and the photo response studies are performed. The thin film is deposited using pulsed laser deposition method and glancing angle deposition.

We report deposition of dual additive assisted Ta_2O_5 / SiO_2 AR coatings on fused silica substrates through sol-gel and dip coating processes. Ta_2O_5 films prepared using additives exhibit enhanced refractive index and film thickness resulting into elevated LIDT. Optimal results such as ~ 99.6% transmission at 968 nm and LIDT value of ~20 J/cm 2 are achieved for Ta_2O_5 / SiO_2 AR coatings. A comparative study is made between additive free and additive assisted Ta_2O_5 film and role of additive in enhancing the efficacy of the optical performance of the AR coatings is discussed.

TABLE OF CONTENTS

PART II- DEVELOPMENT OF HIGH ENERGY LASER INDUCED DAMAGE THRESHOLD OPTICS

LIST OF FIGURES

LIST OF TABLES

ACRONYMS (if any)

Chapter 1: Introduction

1.1 Anti reflection coatings

1.2 Applications

1.3 Anti reflection for high power lasers

1.4 High Laser Induced Damaged Threshold

1.5 Objective

1.6 Outline

Chapter 2: Literature Review

2.1 Anti reflection coatings

2.2 Laser Induced Damaged Threshold

2.3 Ta_2O_5 and SiO_2

2.4 Deposition Techniques

Chapter 3: Experimental setup

3.1 Sol gel

3.2 Dip coating and spin coating

Chapter 4: Characterization techniques

4.1 Transmission spectroscopy for band gap estimation

4.2 Reflectivity

4.3 Ellipsometry

Chapter 5: Observations and results

Chapter 6: Conclusions and Scope for Future Work

REFERENCES

PART I

LIST OF FIGURES

LIST OF TABLES

ACRONYMS

Zinc Oxide	ZnO
Ultraviolet	UV
Atomic Force Microscopy	AFM
Visible	VIS
Pulsed Laser Deposition	PLD

Chapter 1

Introduction

Visible blind Ultraviolet photodetectors-

Photodetectors are devices that detect and measure light, converting it into an electrical signal. They are commonly used in applications like cameras, light sensors, and optical communication systems.

Visible blind UV photodetectors, as the name suggests, detect radiation in the UV region and avoid the detection of radiation in the visible band.

Applications

Applications of Photodetectors

- Cameras: Used in digital cameras to capture images by converting light into electrical signals.
- Light Sensors: Employed in automatic lighting systems to adjust brightness based on ambient light.
- Optical Communication: Used in fibre optic systems to convert light signals into electrical signals for data transmission.
- Medical Devices: Utilized in devices like pulse oximeters to measure light absorption in blood.
- Industrial Automation: Used in sensors for presence detection, colour detection, and quality control.

Applications of Visible Blind UV Photodetectors

- UV Light Detection: Specifically designed to detect ultraviolet light, useful in applications such as UV sterilization and water purification.
- Scientific Research: Employed in spectroscopy and chemical analysis to study materials that fluoresce under UV light.
- Security Systems: Utilized in detection systems for UV light sources, such as those found in counterfeit detection.

Pulsed Laser Deposition:

To date, various methods have been developed and reported for synthesizing ZnO nanostructures, including hydrothermal methods, electro-spinning, chemical bath deposition, electrochemical deposition, and pulsed laser deposition (PLD). Pulsed laser deposition is a thin film

deposition technique, particularly successful in producing highly crystalline structures compared to other techniques.

High-energy laser pulse strikes a target material, causing it to ablate and form a plume of vaporized material. This vapor then deposits onto a substrate, forming a thin film.

PLD allows for precise control over film composition and thickness, making it fit for a variety of materials, including metals and complex oxides.

Glancing angle deposition technique:

Glancing Angle Deposition (GLAD) is a physical vapor deposition technique used to create thin films.

By adjusting the deposition angle and rate, as well as the substrate temperature, researchers can manipulate the film's morphology, resulting in structures like nanorods, nanowires, or porous films.

PLD is known to produce highly crystalline samples. On the other hand, GLAD assists in the formation of pores during the deposition. Thus, the crystallinity, as well as porosity in the grown nanostructures, can be realized by the combinatorial effect of GLAD and PLD.

Interdigitated electrodes

Interdigitated electrodes are different from any other electrode because of their structure and applications.

They have a comb- like structure, interconnected arrangement of the electrodes maximizes the active surface area and also reduces the distance between the two electrodes. These electrodes are suitable for applications requiring fast response time and high speed of operation.

Since the structure is very small and precise, photolithography is used to fabricate the electrode on the thin film sample. There are two ways in which it can be carried out- lift off method and etching. Lift off method provides further advantages- we can make changes in the design and comfortably fabricate the electrode much faster than during etching.

Chapter 2

Literature Review

1. Visible blind UV photodetectors

(Das, 2023) [5]

"Visible-blind" UV detectors are required to have a higher responsivity in the UV range than in lower energy ranges. The cut-off of a visible-blind detector is thus at a wavelength shorter than 400 nm. Detectors with a cut-off below 280 nm could be defined as solar-blind because they respond only to UV radiation with wavelengths shorter than the solar radiation that can penetrate the atmosphere of the Earth.[6] (Sch¨uhle)

2. Ga doped Zinc Oxide film

Highly oriented, aligned and ordered ZnO nanostructures attracted huge attention of the scientific community due to their fundamental properties and potential device applications which shows incredible performance. [1] (SONI, 2020)

It is easy to dope Ga impurity in the ZnO lattice without much lattice distortion. Besides, this does not lose its attractive optical and electrical properties after fractional Ga doping. It is an effective n-type dopant in ZnO, which helps to increase the electrical conductivity by increasing the carrier density. The earlier reports suggested that Ga doping in ZnO significantly enhanced the field emission (FE) properties and it is found to be the most suitable for UV photo-detection and FE-based device applications. [3] (al, 2020)

Primary requirement for developing visible blind UV detectors is semiconductors that have wide bandgap so as to not respond to visible light. Mg O, which is an alloy of insulator MgO and wide bandgap semiconductor ZnO, is a suitable material in this regard.[5] (Das, 2023)

Zinc oxide (ZnO) is an n-type II–VI semiconductor and has a stable hexagonal wurtzite structure with lattice spacing a =0.325nm and c = 0.521 nm. Owing to its direct wide band gap (~3.3 eV at 300K) and large exciton binding energy (~60meV) it is a transparent conducting oxide with applications in thin film transistors and optoelectronic devices such as solar cells, ultraviolet (UV) light emitting diodes (LED). [7] (Ankit Soni, 2019)

3. Glancing angle deposition

The glancing angle geometry in PLD setup assists in the formation of vertical porosity

during the growth process, which helps the deeper penetration of light. The glancing angle deposition (GLAD) produces porous nanostructures by the effect of shadowing during the growth process.[2] (Ankit Soni K. M., 2020)

4. Pulsed laser deposition

Till now, numerous methods have been developed and reported for the synthesis of ZnO nanostructures, e.g. hydrothermal method, electro-spinning, chemical bath deposition, electrochemical deposition, pulsed laser deposition (PLD) etc. [2] (Ankit Soni K. M., 2020)

Usually, the samples grown by PLD are crystalline in nature while the samples prepared by other methods, as mentioned above, have either low crystal quality or polycrystalline nature.[7] (Ankit Soni K. M., 2019)

The glancing angle deposition (GLAD) technique in combination with PLD can help produce the highly porous as well as crystallographically oriented nanostructures. Further, this technique also provides flexibility on the shape and size of nanostructures by tuning the various deposition parameters.[1] (SONI, 2020). The PLD is noteworthy as it produces highly crystalline nanostructures. Moreover, the glancing angle geometry in PLD setup assists in the formation of vertical porosity during the growth process, which helps the deeper penetration of light. The glancing angle deposition (GLAD) produces porous nanostructures by the effect of shadowing during the growth process.[2] (Ankit Soni K. M., 2020)

Chapter 3

Experimental and Characterization

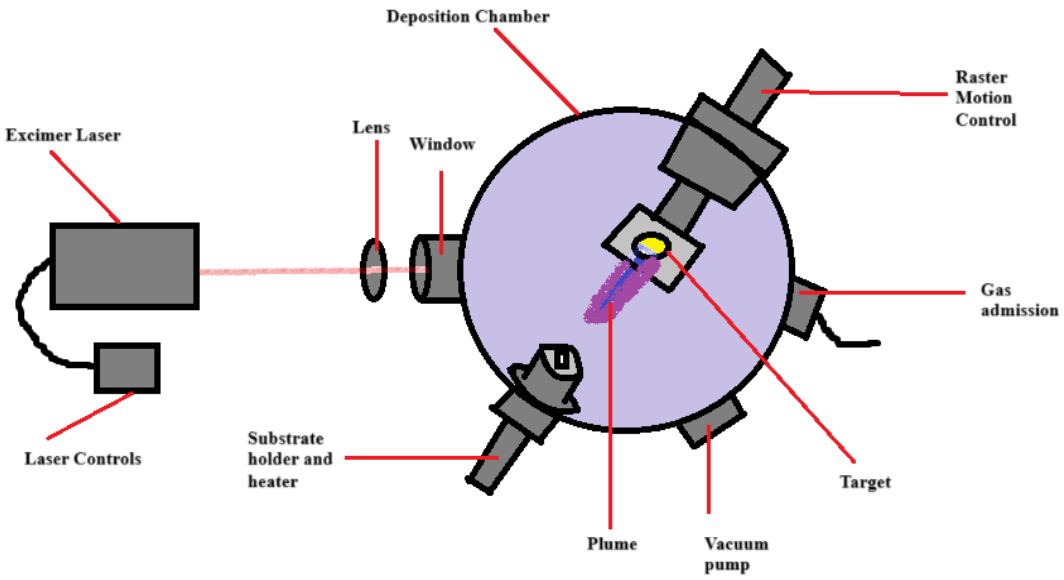

Fig.3.1 Pulsed laser deposition setup

A pulsed laser deposition system consists of the following components-

- Deposition Chamber- A vacuum chamber which has a predefined value for the vacuum pressure as well as oxygen partial pressure
- Laser- High power KrF excimer laser is used for ablating the target material.
  Laser specifications- Wavelength-248 nm, frequency- , fluence-, repetition rate-
- Substrate holder and heater- It holds the substrate on which the film is to be deposited. Heating ensures proper adhesion of the film.
- Rotary Motion Control- The uniformity of deposition depends on the speed of rotation of the target.

Before doing anything in the pulsed laser deposition setup, the substrates need to be properly cleaned. The quartz substrates were sequentially cleaned using acetone and propanol for 10 minutes each in an ultrasonic cleaner before loading into the deposition chamber

The laser beam enters the deposition chamber through a window after passing through a focusing lens. The parameters of the beam and the chamber, such as energy of the laser, pressure inside the chamber, the oxygen partial pressure, voltage, target to substrate distance, base pressure, substrate temperature, number of laser shots fired repetition rate are noted.

After entering the chamber, the laser hits the target material, which is 2% Ga doped ZnO

pellet in this case, and laser ablation occurs. The signature violet blue flame of ZnO can be seen. The plasma formation occurs and the vapor get deposited on the substrate attached on the substrate holder. The substrate is kept at a definite temperature which also influences the quality of the film being formed. The metal-oxide materials are deposited with supplying an oxygen gas into the deposition chamber.

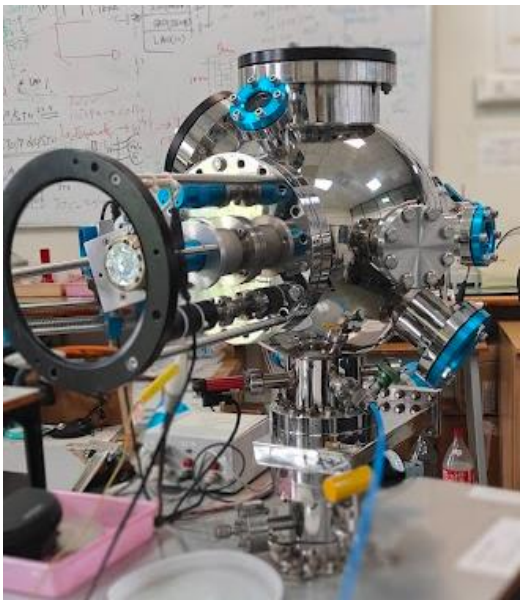

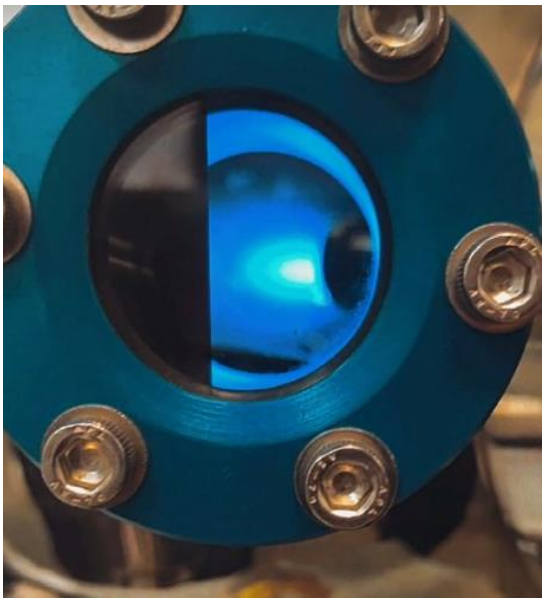

Fig.3.2 and **Fig.3.3** The pulsed laser deposition system at Thin Film Laboratory, SIC, IIT Indore. Inside the chamber we observe the violet blue flame, signature for ZnO plasma

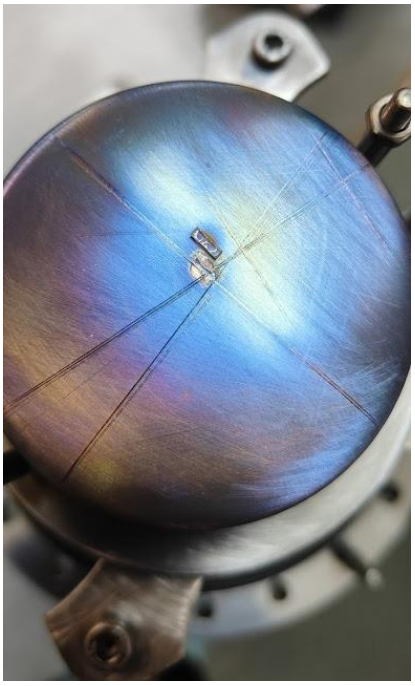

Fig.3.4 Quartz substrate after ZnO thin film deposition

Two thin film and two nanostructure samples were made. The nanostructure samples were made through the glancing angle deposition technique.

- **technique.**

Sample	Pressure (mbar)	Voltage (kV)	T-S	Base pressure	No. of shots	O_2 PP	Rep rate
1	3338	22.6	4.5	$1.2X10^{-3}$	1280	26	4
2	3346	23	4	$8X10^{-4}$	4000	15	10
3	3335	25.1	4.5	$1.3X10^{-3}$	1280	26	4
4	3337	26.4	4.5	$4X10^{-4}$	960	26	4
5	3332	27	4	$1.3X10^{-3}$	4000	15	10
6	3335	29.1	4	$5.4X10^{-4}$	3000	15	10

Table 1. The nanostructure samples made through the glancing angle deposition

- **UV VIS Spectroscopy to determine the nature of bandgap and estimation of bandgap**

UV VIS Spectroscopy to determine the nature of bandgap and estimation of bandgap
Direct bandgap semiconductor- maximum energy of the valence band occurs at the same value of momentum to the minimum in conduction band energy
Indirect bandgap semiconductor- maximum energy of the valence band occurs at the same value of momentum to the minimum in conduction band energy.

Beer Lambert law- $I_t=I_o\ e^{-\alpha d}$
α= absorption coefficient
d = thickness of the sample
I_t, I_o= transmitted, incident light
$\alpha(cm^{-1}) = 2.303A/d$, $A=\log (I_o/I_t) = 2.303 \log(1/T)$

Direct band gap materials also exhibit sharp rise in absorption above the E_g in the plot of energy of light source of UV VIS setup vs absorption coefficient. Direct bandgap materials show high absorption and sharp rise in α^2 vs E

For direct bandgap materials- $\alpha= C[hv-E_g]^{0.5}$
For indirect bandgap materials- $\alpha= C\ [hv-Eg\ -/+\ Ep]^2$
Other electronic transitions such as transition between band and impurity level manifest as shoulder in absorption data.
Plot-

i. α vs E
ii. α^2 vs E
iii. $\sqrt{\alpha}$vs E
iv. αx E vs E
v. $(\alpha \times E)^2$ vs E
vi. $\sqrt{\alpha \times E}$vs E

(Jaramillo, 2017)

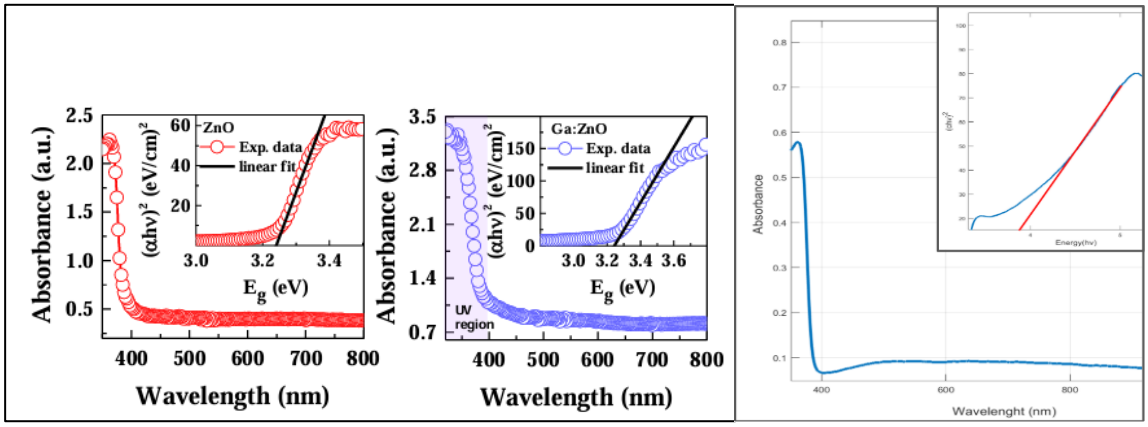

Fig.3.5 UV VIS Spectroscopy to determine the nature of bandgap and estimation of bandgap (SONI, 2020)

- **Atomic force microscopy**

It is used for imaging friction between surfaces, elasticity of materials, electrical forces, magnetic forces, conductivity, surface potential etc.

An AFM scans a sample using a sharp tip mounted on a flexible cantilever. As the tip is near the surface:

- Attractive forces pull the cantilever downward
- Upon contact, repulsive forces dominate, pushing cantilever upward

A laser beam reflects off the cantilever onto a position sensitive photodetector. Even nanoscale deflections alter the laser's path, allowing the position sensitive photodetector to track height variations, force interactions etc.

Standard imaging techniques: (Park systems, 2025)

Contact Mode	Non-Contact Mode	Tapping Mode
• The most basic mode of Atomic Force Microscopy for measuring the physical characteristics of the surface. • The cantilever scans while applying a constant force onto the surface of the sample. • As the tip approaches close to the sample, the tip eventually contacts the surface. Once engaged, the cantilever bends upwards proportional to the amount of applied imaging force. • The deflected laser spot on the position sensitive photo detector will move due to the change in contact force.	• The cantilever oscillates just above the surface as it scans. • A high-speed feedback loop prevents the cantilever tip from crashing into the surface. • As the tip approaches the sample surface, the oscillation amplitude of the cantilever decreases.	• The cantilever again oscillates just above the surface, but at a much higher amplitude of oscillation. The bigger oscillation makes the deflection signal large enough for the control circuit, and hence an easier control for topography feedback.

- **Table 2. Standard imaging techniques in Atomic Force Microscopy**

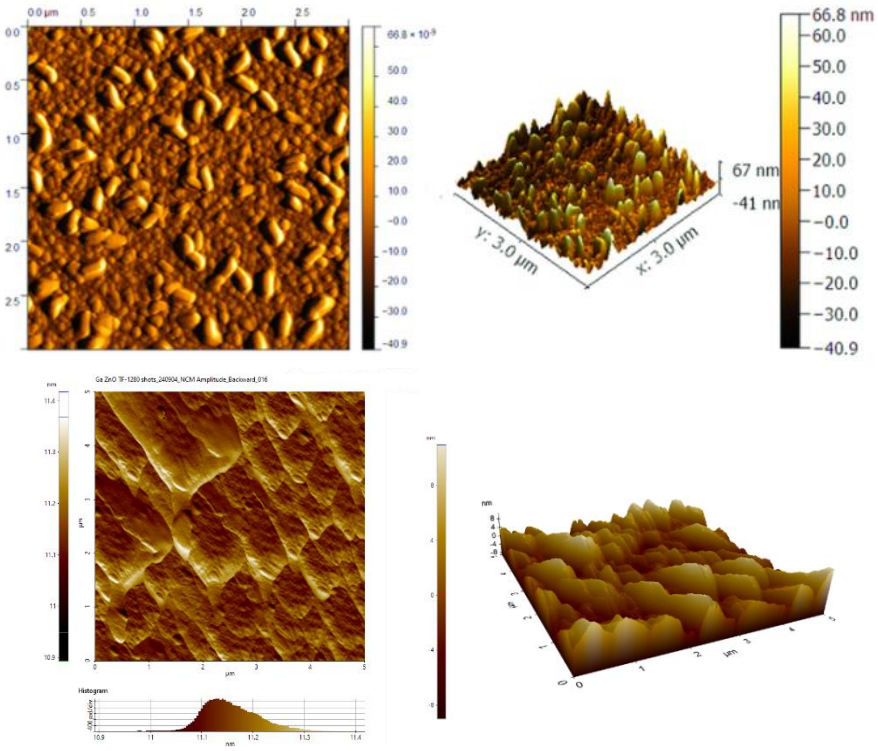

Fig. 3.6 Atomic force microscopy for ZnO film

- **X Ray diffraction**

When X-Rays enter a crystal, each atom behaves as a diffraction point, and the whole crystal behaves like a 3-D grating. The obtained diffraction pattern provides information about the internal arrangement of atoms in the crystals, which helps to determine the crystal structure.

Constructive interference occurs between the diffracted waves if the following Bragg relation is satisfied,

$$2d \sin \emptyset = n\lambda$$

d is the inter-planer distance, θ is the incident, n is a positive integer and λ is the X-ray wavelength. When the above criterion is fulfilled, a peak in the diffraction pattern appears at a particular angle. It is noteworthy that the XRD pattern of each material is different and unique, which validate the purity of the structural phase of that material.

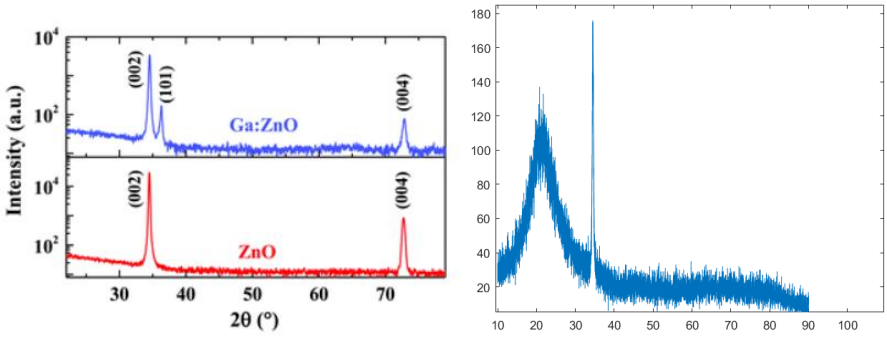

Fig. 3.7 XRD patterns for ZnO films (SONI, 2020)

Chapter 4

Fabrication of electrodes

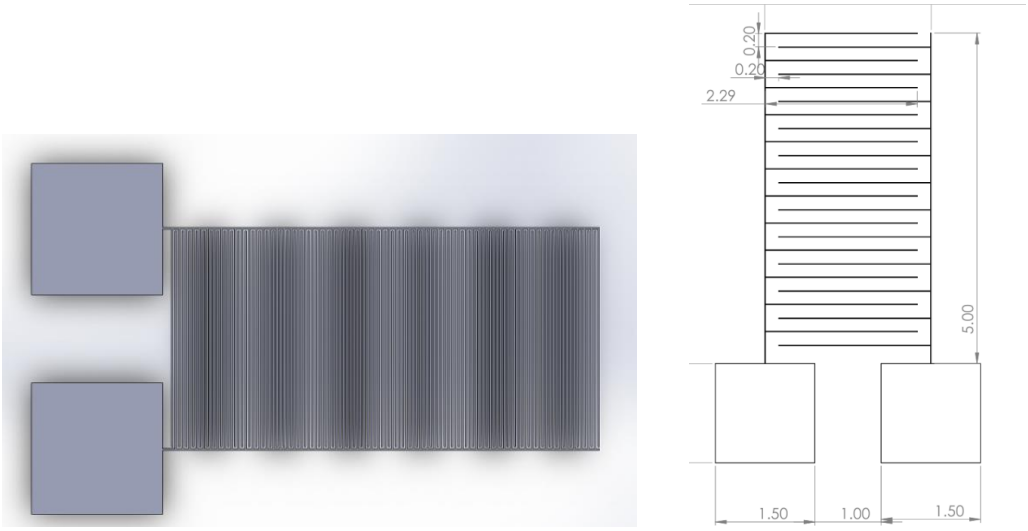

Fig. 4.1 CAD design for the electrode

Photolithography is a manufacturing process used to fabricate integrated circuits. The process involved is as follows:

- A photoresist is applied to the thin film sample
- A mask containing the pattern of the electrode is placed over the photoresist layer.
- Light, usually UV radiation, is used to transfer this pattern on the thin film. Detailed procedure is given further in the text.
- The areas exposed to the radiation undergo a chemical change which makes the exposed photoresist soluble in a developer solution.

Advantages of photolithography: Very small shapes and patterns can be fabricated, precision and control over the shape and size, the patterns are created on the sample in a single step

Lift off method:

This technology is a method of creating patterns on a sample surface using a photoresist. A photoresist is a light sensitive material that changes in chemical composition when exposed to radiation. Structures ranging from nanoscales to micrometer dimensions can be fabricated.

Reverse of lift off process. Material is chemically removed from the surface of the sample. Areas on the sample are protected by a masking material and an etchant is used to remove

the remaining material. The masking material can also be a photoresist. For the current work, we made use of lift off method, as it is more mobile compared to etching. It is faster and also provides flexibility in changing the dimensions of the mask.

Procedure:

- The sample- Ga:ZnO on quartz is cleaned in an isopropyl alcohol and acetone baths
- The sample is coated with a photoresist using a spin coater. The pressure and speed inside are kept constant. The photoresist is poured on the sample then the spin coater is started.
- A mask containing the pattern of the interdigitated electrode is placed over the photoresist coated samples.
- Ultraviolet radiation source is placed above the sample, exposing the photoresist in areas other than the part covered with the mask.
- The area exposed to the UV light undergoes a chemical change, making it soluble in a developer solution.
- The sample is heated or baked at 110^0C after developing.
- The exposure reaction- The radiation turns the polymer soluble in the basic developer solution by creating acid.
- AZ developer is a sodium-based solution used to develop photoresists. Photoresist is removed using this developer. The electrode pattern stays on the sample with everything else washed away due to the developer.
- All the procedures related to the mask fabrication for the gold electrodes were carried out with the help of the Synchrotrons Utilization Section and the Free Electron Laser & Utilization Section at RRCAT Indore.

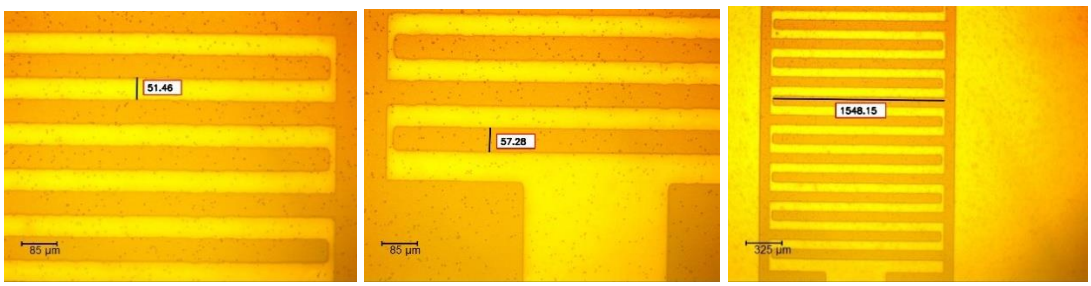

Fig. 4.2 Microscopic images of the gelatin mask

Gold deposition:

Thin layers of Chromium (15nm) and Gold (60nm) were deposited using table top gold sputtering unit at the Optical Coating Facility, High Energy Lasers and Optics Section, RRCAT Indore. Gold was coated on the entire substrate and lift off was performed by ultrasonication in acetone.

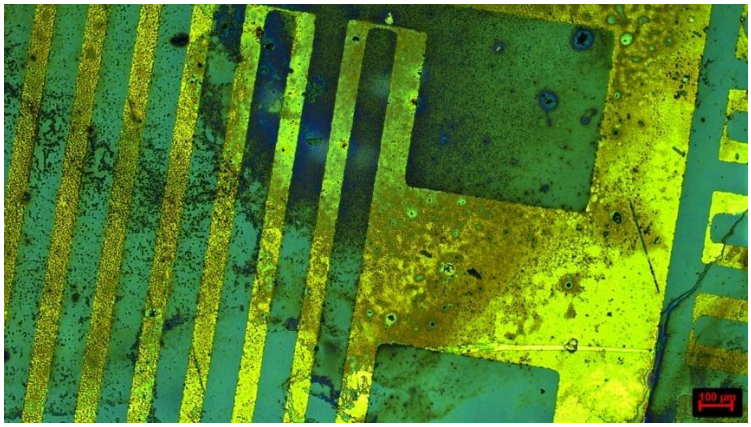

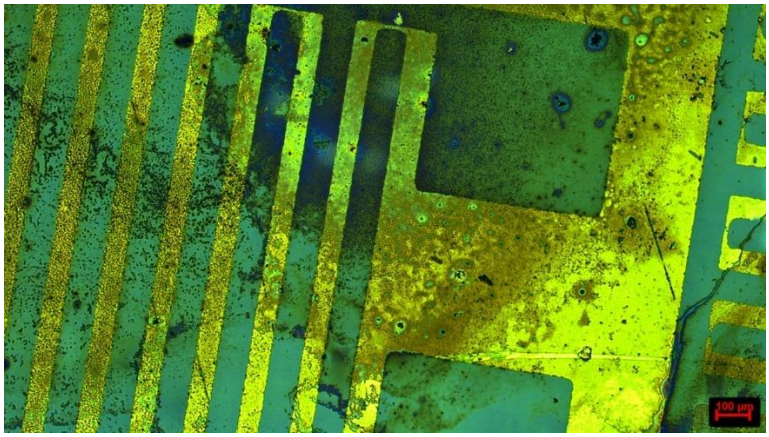

Fig. 4.3 and **Fig. 4.4** Microscopic images of the gold electrodes after lift off

Chapter 5

Observations and Results

In the present chapter, the results of the characterization techniques performed are discussed. The bandgap estimation and analysis of optical properties are performed through the UV-Visible spectroscopy. The crystallinity is verified through the means of X-ray diffraction. The surface morphology and other parameters such as roughness is verified through atomic force microscopy. At last, the film's response to UV radiation is observed by performing the photo response studies in dark surroundings as well as under UV radiation.

In summary, the characteristics of the thin film deposited through the pulsed laser deposition as well as the glancing angle deposition are studied, and it has been verified that the parameters during the deposition influence different characteristics such as surface morphology, crystallinity and even the photodetection properties.

Sample	Pressure (mbar)	Voltage (kV)	T-S	Base pressure	No. of shots	O_2 PP	Rep rate
1	3338	22.6	4.5	$1.2X10^{-3}$	1280	26	4
2	3346	23	4	$8X10^{-4}$	4000	15	10
3	3335	25.1	4.5	$1.3X10^{-3}$	1280	26	4
4	3337	26.4	4.5	$4X10^{-4}$	960	26	4
5	3332	27	4	$1.3X10^{-3}$	4000	15	10
6	3335	29.1	4	$5.4X10^{-4}$	3000	15	10

Table 3. The nanostructure samples made through the glancing angle deposition

5.1 UV Visible spectroscopy- Band gap calculations

The UV spectroscopy reveals significant insights into the optical properties. By using UV spectroscopy, we calculate the absorption coefficient after getting the transmission data by using the following formula-

Beer Lambert law-

$$I_t = I_o\, e^{-\alpha d} \text{ , which implies } \alpha\ (cm^{-1}) = \frac{2.303A}{d},$$

$$A = \log (I_o/I_t)$$

$$= 2.303 \log \left(\frac{1}{T}\right)$$

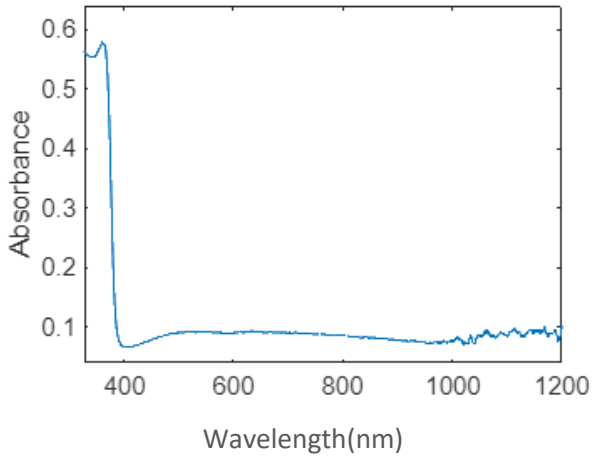

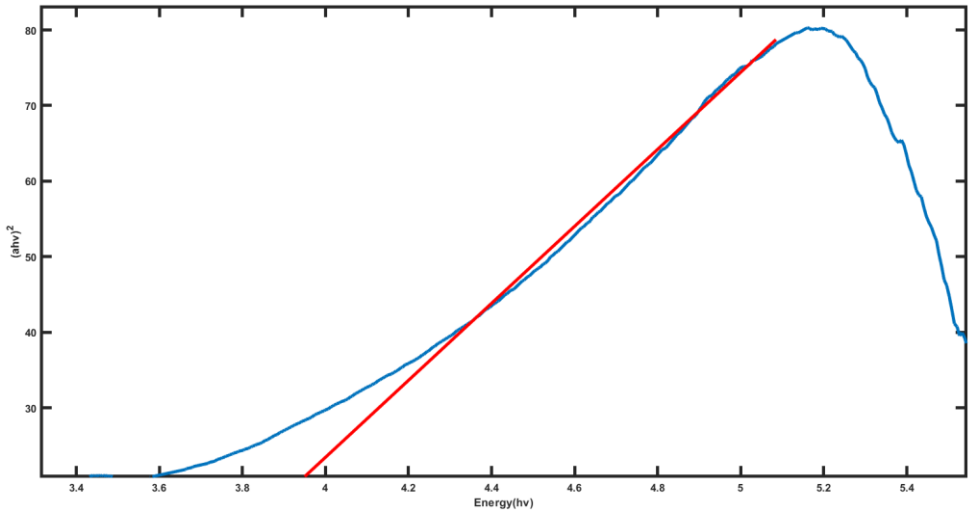

Fig 5.1 and **Fig 5.2**. - UV spectroscopy for sample 3

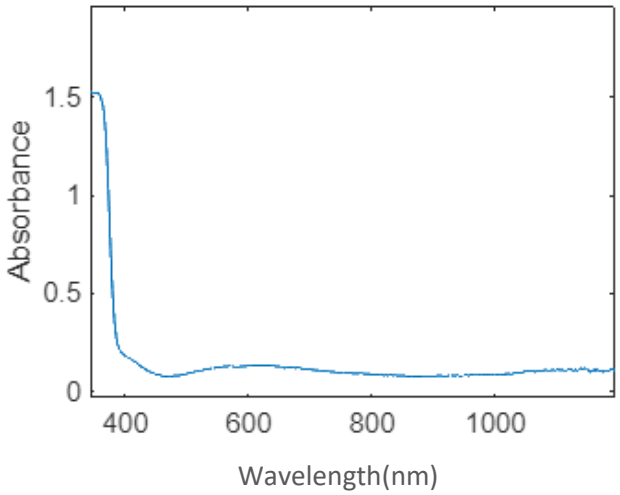

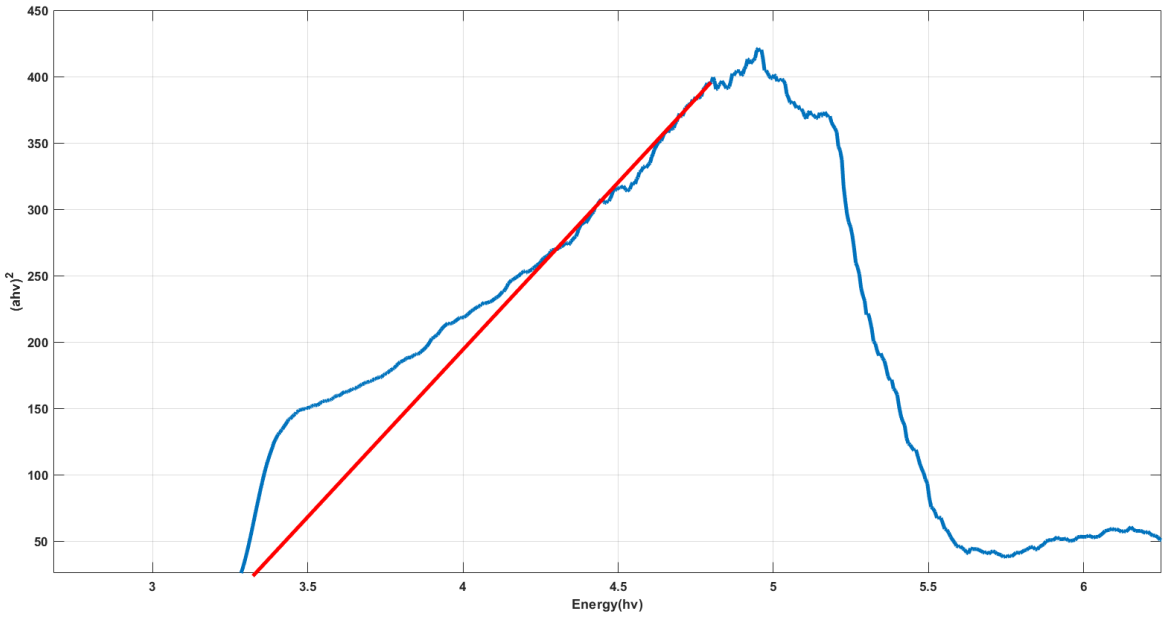

Fig 5.3 and **Fig 5.4**. - UV spectroscopy for sample 4

The plot-(α x E)^{2}vs E gives us the direct energy bandgap for all the samples, which was found to be in the range 3.5eV to 4 eV The first graph of each sample demonstrates a notable absorption edge around 400nm, indicating strong absorption in the ultraviolet region. This behaviour is characteristic of wide bandgap semiconductors, suggesting effective light absorption. The second plot in case of each sample depicts the Tauc plot, used to determine the optical bandgap of the material. By extrapolating the linear portion of the curve, the bandgap energy can be estimated.

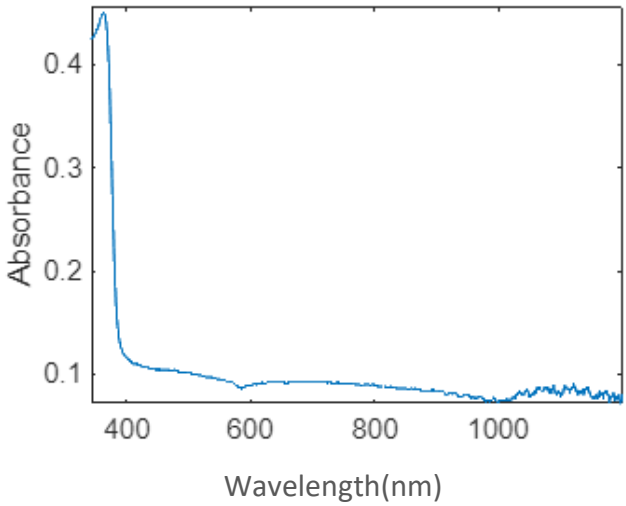

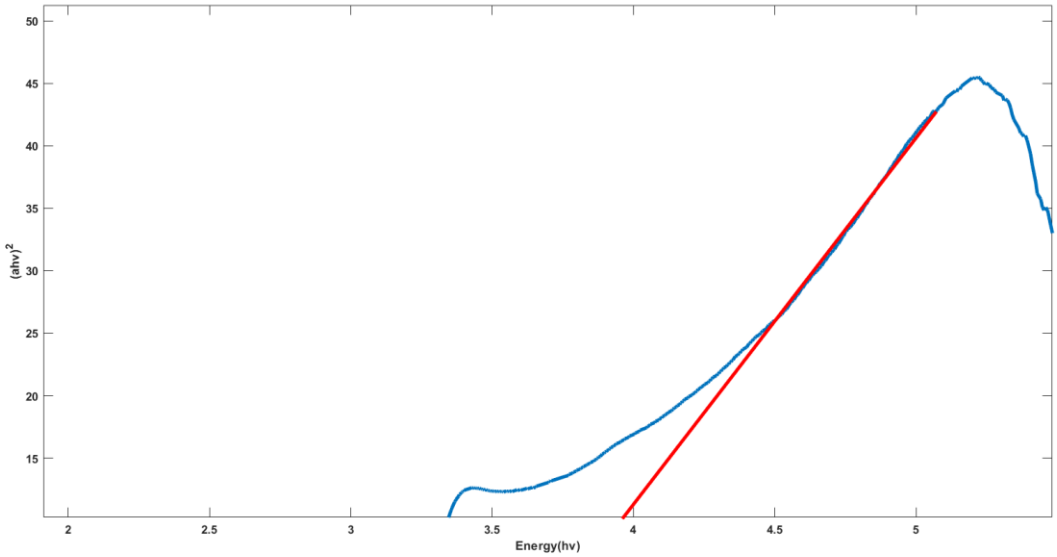

Fig 5.5 and **Fig 5.6**. - UV spectroscopy for sample 5

In case of semiconductors, the most common method of band gap estimation is by analysing the electronic transitions between conduction band and valence band. Energy difference between the conduction band maximum and valence band minimum is called the electronic band gap. Electronic band gap doesn't have to be equal to the optical bandgap of a material. We can estimate the value of the optical bandgap. In addition, through UV-Visible spectroscopy, we can calculate direct or indirect bandgap- either one which is not forbidden for a material. The calculated bandgap energy is essential for understanding the material's suitability for specific applications. (al, 2020)

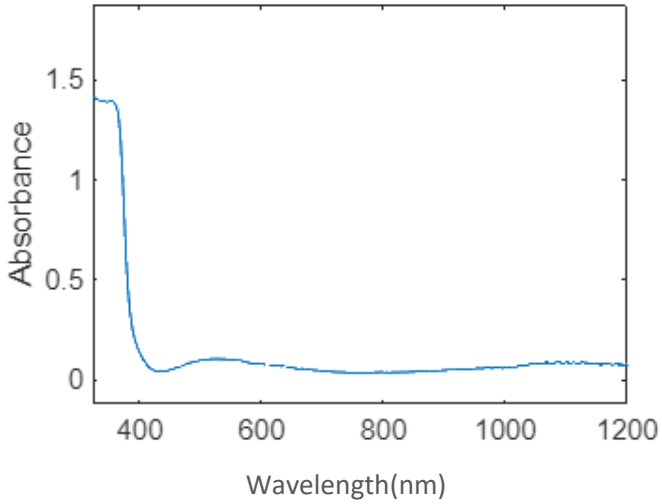

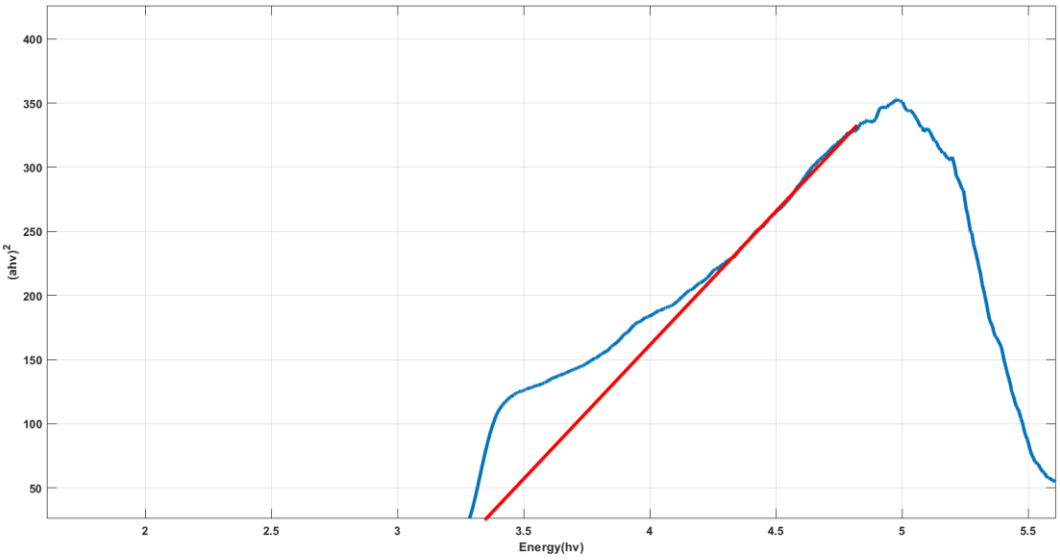

Fig 5.7 and **Fig 5.8**. - UV spectroscopy for sample 6

The bandgap energy so calculated is important to understand the material's suitability for very specific applications- for example photovoltaic cells, LEDs etc

Overall, these results show that Ga:ZnO thin films possess favourable optical characteristics for various optoelectronic devices.

5.2 Atomic Force Microscopy

The Atomic Force Microscopy images provide detailed insights into the surface morphology and topography at the nanoscale. The first image for each sample indicates a surface with distinct features, showing a uniform structure with peaks and valleys.

The height varies from 10.9 nm to 11.3 nm, suggesting a smooth surface, which is advantageous for electronic applications where surface roughness can impact a device's performance.

The histogram accompanying the images show height distribution centered almost around 11nm, with the peak frequency indicating a consistent surface profile.

The uniformity, along with a root mean square roughness is quite low which is an indication towards the structural integrity of the film samples.

The AFM micrographs show a relatively smooth surface with the presence of small peaks and valleys-indicating a very well-defined topography. The average height of around 11.1 nm suggests a uniform surface. If we consider all the sample graphs, the variation is mainly between 11.2 nm,11.4nm, 11.6nm and 11.9nm. The low RMS value can be interpreted from the narrow height distribution which indicates minimum surface irregularities.

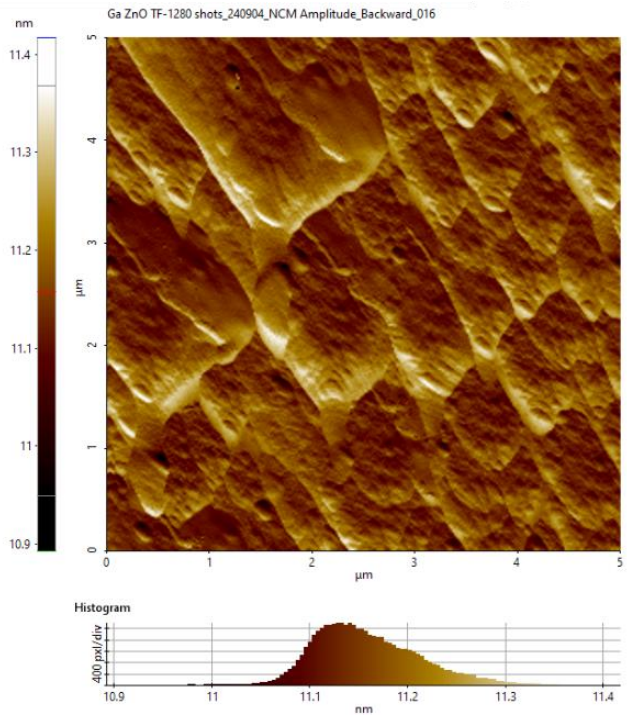

Fig 5.9 AFM micrographs for sample 3

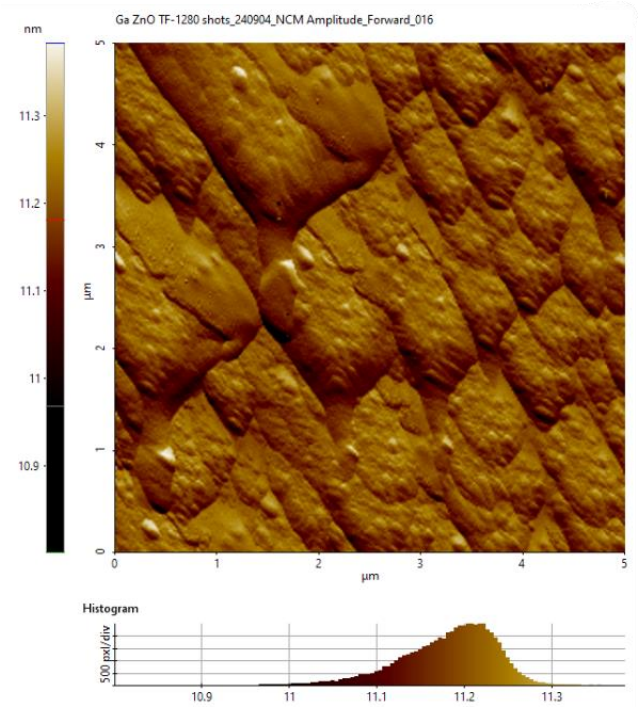

Fig 5.10. – AFM micrographs for sample 3

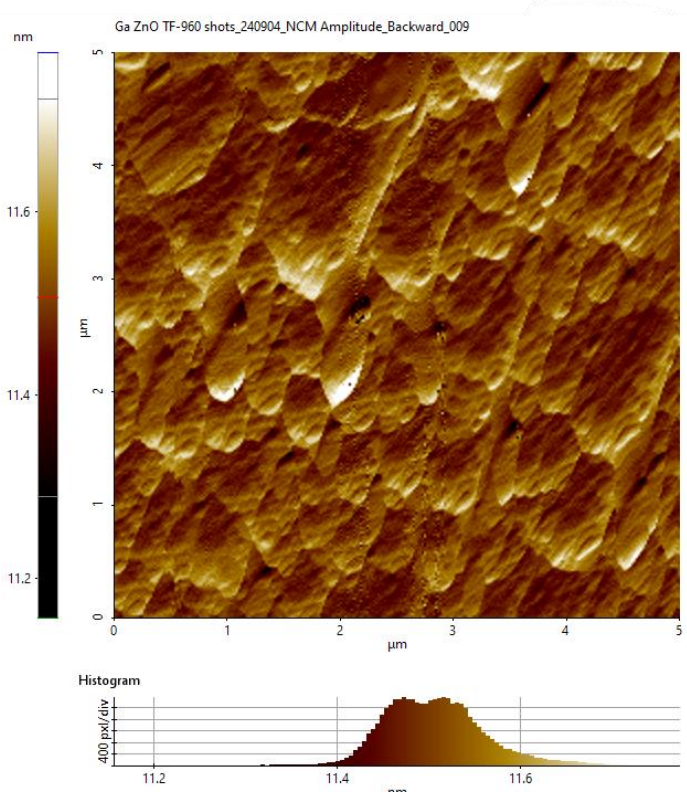

Fig 5.11 – AFM micrographs for sample 4

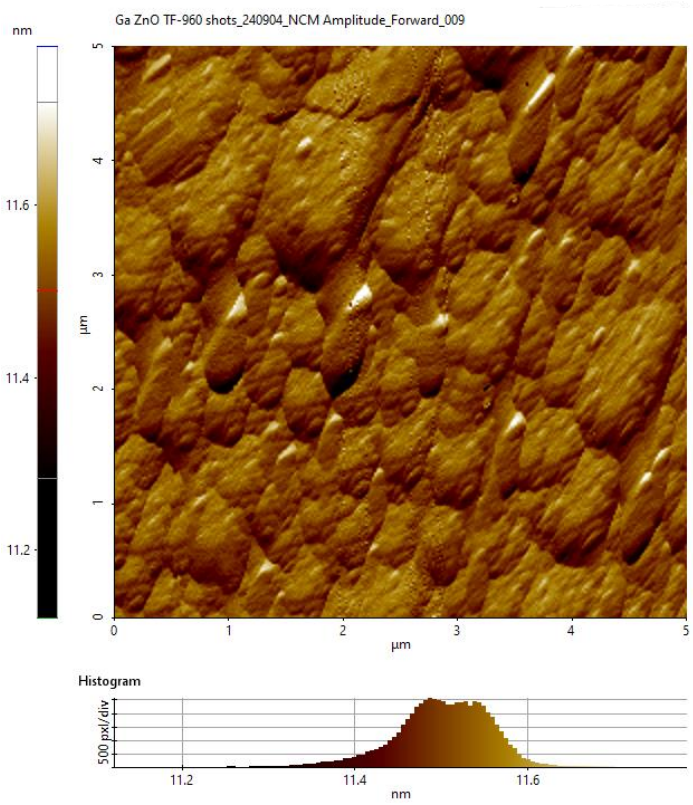

Fig 5.12. – AFM micrographs for sample 4

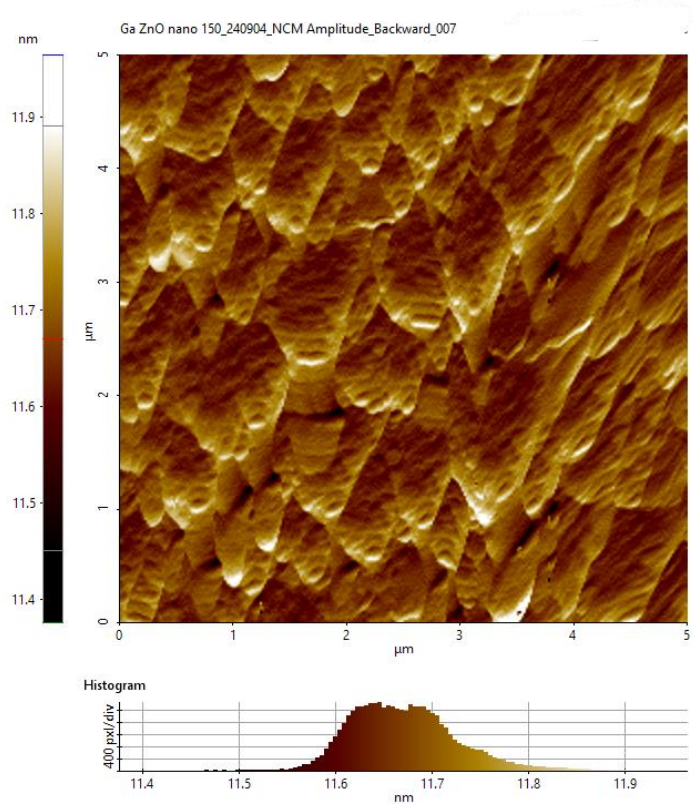

Fig 5.13 – AFM micrographs for sample 5

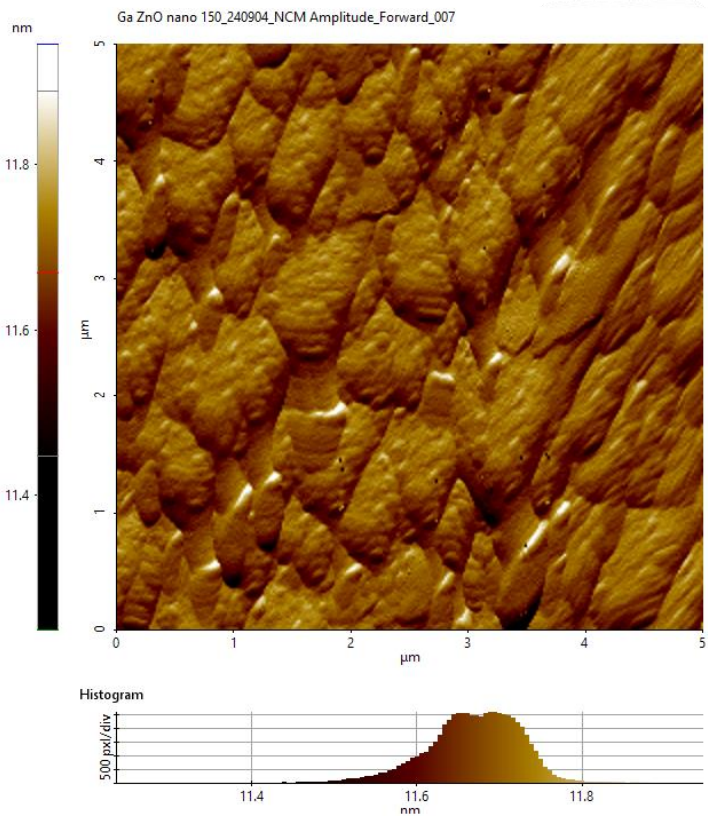

Fig 5.14. – AFM micrographs for sample 5

Sample number 5 shows a lesser rugged surface than sample number 4, with smoother transitions bin between features. The height variation is between 11.4nm to 11.8nm.

In summary, the AFM micrographs show that the film samples have favorable surface properties, with high uniformity and low roughness. These parameters are critical for improving the performance of many devices in advanced technological applications. Smoothness of the film ensures minimum scattering losses in optoelectronic devices. The low roughness might also improve surface interactions, which could prove beneficial in applications such as sensors and photocatalysts. A reduction in roughness can also improve charge transportation in electronic devices.

5.3 X-ray Diffraction

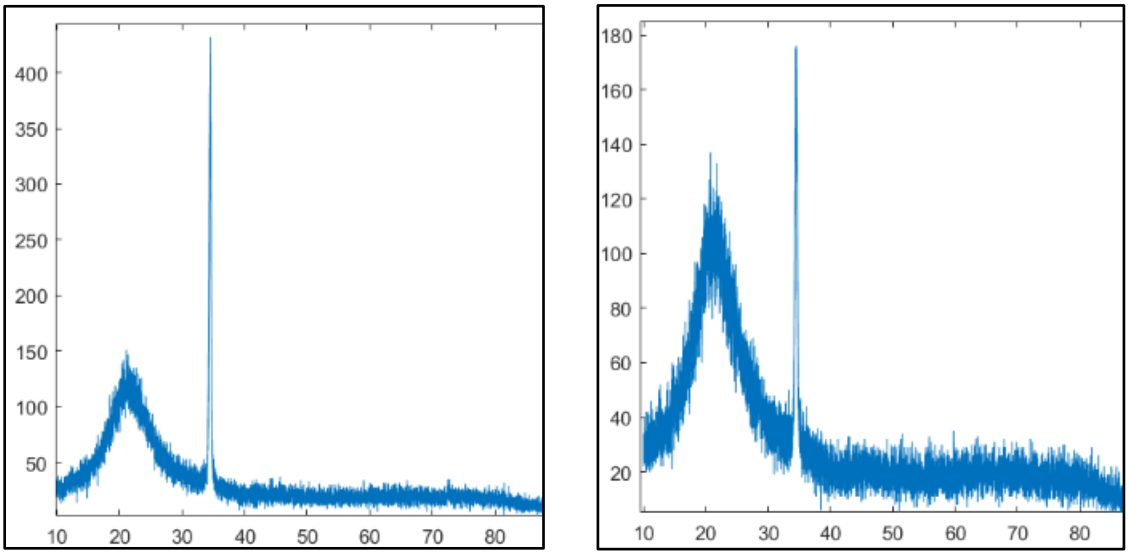

Fig 5.15. -2θ≈ 31.09° and 34.5° represents (100) and (002) peaks, respectively for ZnO crystal planes.

X-Ray diffraction patterns of two samples are shown. These provide valuable information about the crystallinity and the phase composition of the material in use. The first spectrum displays a significant peak of about 450 counts at around 2θ=34.5°, indicating the 002 crystallographic plane of ZnO wurtzite structure, and also indicating high crystallinity.
The second spectrum also shows similar readings, in addition with a slightly higher intensity and broader peak which is a probable indication of increased defect density and other variations in crystal structure. The following insights can be obtained-

First sample depicts a higher crystallinity, which can be positive for applications in transparent and conductive oxides, sensors etc. In comparison, the second sample has a more complex microstructure and hence the performance can be affected. The broader peaks indicate low crystallinity and the presence of amorphous material.

In summary, these patterns highlight the crystallinity and the structural integrity of the thin film samples. The difference in peak intensity and breadth may inform future optimization efforts in the synthesis process.

5.4 Ultraviolet photodetection studies

For the transient photo response studies, the sample with and without thew electrodes were considered. The voltage was provided to both the samples and the current values were observed in the dark and under ultraviolet radiation.

The following procedure was followed to make the observations:

- The electrodes were placed in a dark room and the value for dark current was noted. This is the value of the saturation current that is obtained after switching on the UV light as well as when the electrodes are kept in the dark for sufficient amount of time.
- As the UV radiation is turned on, there is a steep increase in the value of the current. The values are taken until a constant value is obtained.
- After a constant value is obtained the UV radiation is turned off. This cycle is repeated again. The increase and decrease is due to absorption and de-absorption of oxygen molecules by ZnO.

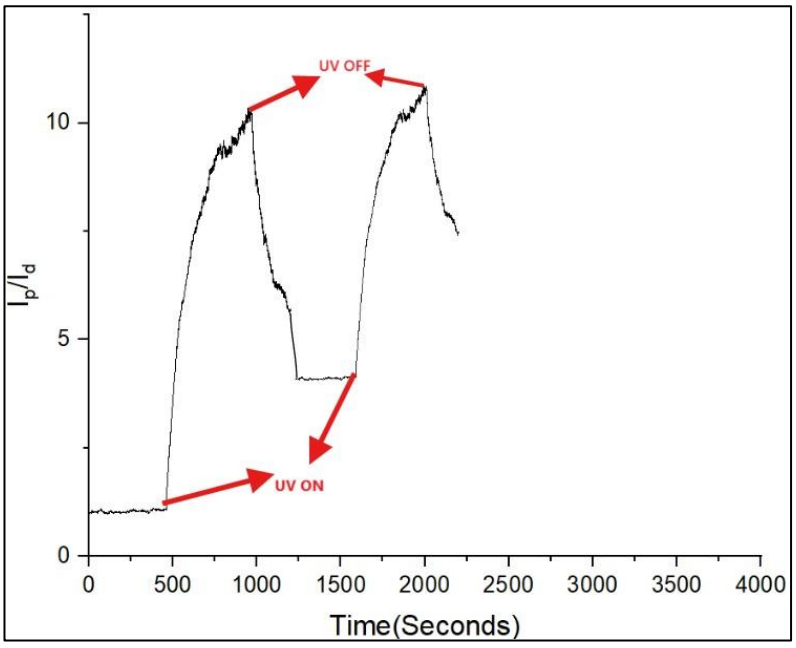

Fig. 5.16- Photoresponse studies performed for thin film sample. Arrows indicate the moment UV is turned ON and OFF

Observations- (Table 4)

Sample	Dark Current (µA)	Photo-to Dark Current ratio
Ga:ZnO (0.1V)	0.13285	10.16
Ga:ZnO (1V)	26.206	1.6

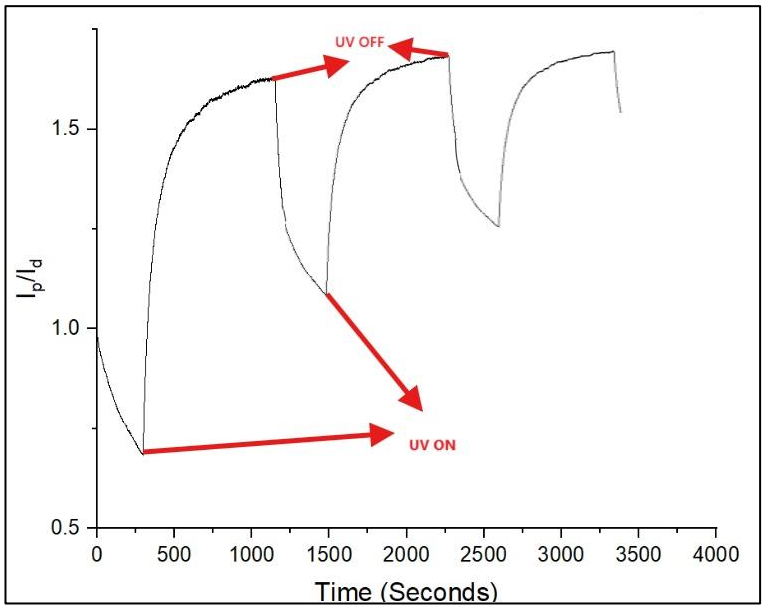

Fig. 5.17 - Photoresponse studies performed for thin film sample

The time resolved photo response characteristics of the thin film samples were observed under periodic ultraviolet light illumination. The photocurrent, that too at different applied voltages, was monitored as a function of time. Initially, the current remains constant- this is an indication of the low as well as stable dark current. After the first exposure, the device showed a sharp increase in the I_p/I_D ratio, depicting a strong and rapid photo response. When the light was turned off, the current value decreases almost to the value of dark current.
The device exhibits a sharp increase in I_p/I_D upon UV illumination at around 500 seconds, indicating a good response to UV radiation. The current ratio quickly rises from the dark current value, also known as the baseline to a peak value of 10.16, indicating an enhancement in the conductivity due to photoexcited charge carriers. The values of dark current in both the graphs are 0.1328 and 26.206 μA at voltages 0.1V and 1V respectively.

The second graph indicates a moderate photo response, with the ratio rising from 0.6 to a value of almost 1.7. The signal dynamics are quite rapid and are also reproducible over multiple cycles. Such samples, as proven by the graphs, are ideal for applications requiring rapid switching and low persistent efforts.

These results show the efficacy of the doping of Ga as well as the use of pulsed laser deposition in enhancing the optoelectronic properties of ZnO films. The high I_p/I_D ratio, stable switching behavior and low dark current values substantiate the material's potential.

Chapter 6
Conclusions and Scope for Future Work

To conclude the work- visible bling UV photodetectors fabricated using the pulsed laser deposition and glancing angle deposition method result in highly crystalline as well as very porous structures. The enhancement in such properties is solely due to the combination of these two processes.

Further, the interdigitated structure of the gold electrodes that are used are quite complex to fabricate, but are equally advantageous.

The fabrication of the electrodes is a very complex and sophisticated task. During the lift off stage the electrode can get corroded very easily. A better interdigitated structure is required to properly analyze the effect of these structures.
In theory, an interdigitated structure will be responsible for a much faster response and an enhanced amount of the generated photo current. The reason behind this may be attributed to the decreased distance between two electrode teeth. It would be of great interest these structures and their role in UV photodetection are explored further.

PART II

LIST OF FIGURES

LIST OF TABLE

LIST OF PUBLICATIONS

Dual additive assisted Ta_2O_5/SiO_2 antireflection coatings with high laser induced damage threshold- Shruti Pankaj Sharma [2], Nikita Sharma [3], Suparna Pal [1,3], Rajiv Kamparath [1], V.V.V. Subrahmanyam [1], Neha Sharma [1,3], N. S. Benerji [1]

[1] High Energy Laser & Optics Devision, RRCAT, Indore, [2] Indian Institute of Technology, Indore, [3] Homi Bhabha National Institute, Training School Complex, Anushakti Nagar, Mumbai

Poster presented at the National Laser Symposium-33,

ACRONYMS

Tantalum pentoxide	Ta_2O_5
Silicon dioxide	SiO_2
Laser induced damage threshold	LIDT
Ultraviolet	UV
Anti-reflection	AR
Full Width at Half Maximum	FWHM
Atomic Force Microscopy	AFM
Acetyl Acetone	ACAC
Diethanolamine	DEA

Chapter 1

Introduction

Whenever light travels from one medium to another, a portion of it is transmitted, while a significant amount is reflected. The degree of light reflection can increase depending on the angle of incidence and the refractive index of the new medium. Moreover, some of the light that is reflected from various surfaces can eventually reach the focal plane, resulting in the appearance of ghost images.

Anti-reflection coatings are types of optical coatings that can be applied to surfaces of optical devices to reduce reflection losses.

Working principle of anti-reflection coatings-

The working principle of anti-reflection (AR) coatings is based on the phenomenon of destructive interference of light waves. When light encounters a surface, some of it is reflected while some is transmitted. AR coatings are designed to minimize the reflected light by using thin films of materials with specific refractive indices.

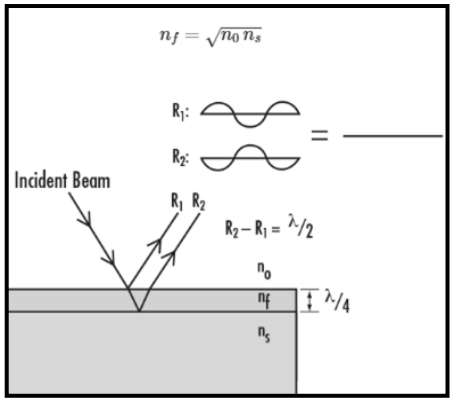

Fig. 1-Principle of anti-reflection coatings

Path difference between two rays-

$\Delta = 2n_f t \cos r$

For normal incidence,

$$\Delta = 2n_f t$$

$$\Delta = 2n_f t = \frac{(2N+1)\lambda}{2}$$

$$N = 0, t = \frac{\lambda}{4n_f}$$

Fresnel's equations for reflectivity at two interfaces-

$$r_1 = \frac{n_o - n_f}{n_o + n_f}$$

$$r_2 = \frac{n_f - n_s}{n_f + n_s}$$

If the system consists of three layers and the thicknesses of the layers are equal to quarter wave thickness at a specific wavelength, the minimum reflection from the coated surface for the normal light is given by-

$$R = \frac{(n_0 n_s n_3^2 - (n_1 n_3)^2)^2}{(n_0 n_s n_3^2 + (n_1 n_3)^2)^2}$$

The condition for the anti-reflecting light to be zero is-

$$\frac{n_1 n_3}{n_2} = \sqrt{n_o} n_s$$

Where n_1, n_2, n_3 are the refractive indices of the layers and n_0, ns are the refractive index of air and the substrate, respectively.

Applications

Anti-reflection (AR) coatings have a wide range of applications across various fields due to their ability to enhance light transmission and reduce glare. Here are some key applications:

1. Eyewear

- Prescription Glasses: AR coatings improve clarity and comfort by reducing glare from screens and bright lights, making them ideal for everyday use.
- Sunglasses: Many sunglasses use AR coatings to minimize reflections from surfaces like water or roads, enhancing visual comfort.

2. Optical Devices

- Camera Lenses: AR coatings reduce lens flare and ghosting, improving image quality in photography and videography.

- Microscopes and Telescopes: Enhanced light transmission leads to clearer images, crucial for scientific research and observation.

3. Displays

- Smartphones and Tablets: AR coatings improve visibility in bright conditions, making screens easier to read outdoors.
- Televisions and Monitors: Used to reduce reflections and enhance the viewing experience, particularly in well-lit environments.

Applications in High-Energy Lasers

1. Laser Components:

   Laser Lenses: AR coatings are applied to lenses in high-energy laser systems to maximize the transmission of laser light, reducing loss and improving efficiency.

   Beam Splitters: Coatings help minimize reflections that can interfere with the laser beam, ensuring more accurate beam splitting and control.

2. Optical Windows:

   Protection and Efficiency: AR-coated optical windows in high-energy laser setups allow maximum light transmission while protecting sensitive components from environmental damage.

3. Amplifiers and Oscillators:

- Improved Performance: In laser amplifiers, AR coatings reduce losses at the input and output interfaces, enhancing overall amplification efficiency.
- Loss of light can impact performance of optical components.
- Chemical and physical properties of substrates can also be protected
- For better feedback, large output power and thermal stability, such coatings are a necessary requirement.
- Absorption of laser radiation leads to increased temperature and a correspondingly higher. This changes the properties of the transmitted laser beam and can therefore impair the performance of the manufacturing process.

- **Limitations**

➢ It is not always possible to find a coating material with a suitable refractive index.

➢A single–layer coating works only in a limited wavelength range.

Laser Induced Damage Threshold for high power lasers

The High Laser Induced Damage Threshold is a critical parameter in the design and selection of optical materials for high-energy laser applications.
Laser-induced damage threshold (LIDT) is defined within ISO21254 as the “highest quantity of laser radiation incident upon the optical component for which the extrapolated probability of damage is zero”.
The Laser Induced Damage Threshold (LIDT) is a critical specification to consider when integrating an optical component into a laser application.
Optical components specified with a Laser Damage Threshold are designed and guaranteed to endure a specific level of laser fluence.

Objective

Sol gel prepared amorphous Ta_2O_5 thin film for application in high LIDT antireflection coating.

Amorphous Ta_2O_5 thin films have been deposited using sol-gel method using tantalum ethoxide as a precursor for application in optical coating for high power laser. Effects of additives into the sol were studied.

Optical properties like bandgap, refractive index and transmission etc. of the additive assisted Ta_2O_5 thin films were measured.

The sol gel prepared Ta_2O_5 film has been used as antireflection coating (AR) on silicon and fused silica (FS) substrate.

Photothermal absorption and surface flatness of the sol-gel deposited films were studied.

Laser induced damage threshold of optical films is one of the major figures of merit which determines the output of high-power laser systems. LIDT of the thin films were measured.

Chapter 2

Literature Review

1. AR coatings in high energy lasers

Loss of light through reflection can impact the performance of optical components in many important applications, and so the primary purpose of anti-reflection coatings are to come as close as possible to eliminating this reflected light [15]. Chemical and physical properties of the substrate can sometimes be protected by AR coatings. For better feedback, large output power and thermal stability, such coatings are a necessary requirement. Absorption of laser radiation leads to increased temperature and a correspondingly higher refractive index of the optics. This changes the properties of the transmitted laser beam and can therefore impair the performance of the manufacturing process [15]. The tiny defects in the optical film will lead to the degradation of the laser beam quality. More seriously, once the optical film is damaged, it will lead to the failure of the whole laser system and directly affect its service life. Therefore, it is of utmost importance to improve the laser damage resistance of optical films and investigate the damage mechanism [25].

2. Laser-induced damage threshold

Laser-induced damage threshold (LIDT) is defined within ISO 21254 as the "highest quantity of laser radiation incident upon the optical component for which the extrapolated probability of damage is zero". The issue of how effective the damage resistance of the films on the output power, stability, and even the life time of laser systems puts laser-induced damage of the films into an important position in the field of high-power lasers [26]. LIDT is obtained by damage probability analysis.

$$F_{th} = \frac{F_{min}(\mathrm{D}) + F_{max}(\mathrm{ND})}{2}$$

Here, the laser damage threshold F_{th} is defined as the mean value of the highest energy density with no damage F_{max} (ND) and the lowest energy density with damage F_{min} (D).

3. Ta_2O_5 and SiO_2

Ta_2O_5 films exhibit relatively low levels of optical and mechanical loss.

Besides these, Ta_2O_5 has found a wide range of application starting from the field of biomaterials to corrosion resistance of alloys [4]. The refractive index and the thickness are controlled by the composition and the concentration of the solution respectively [10]. Although optical constants of Ta_2O_5 are important to the development of EC devices, very few reports have been published on the subject. Therefore, it is important that the optical constants of Ta_2O_5 be investigated and related to the deposition conditions [11].

Tantalum oxide (Ta_2O_5) has useful optical and dielectric properties. It is a fairly stable oxide with an orthorhombic structure, a melting point of 1800^0C and a density of 8.27 g/cm^3. It is moderately hard. It has a refractive index of ~ 2.1. It is an electrical insulator with a high dielectric constant (25-35). Ta_2O_5 can accommodate a wide variety of dopant ions through subtle variations of its crystal structure [18].

Ta_2O_5 films find applications in various fields such as dielectric for storage capacitors, gate insulators in metal-oxide-semiconductor (MOS) devices, optical coatings, anti-reflection coatings and coatings for hot mirrors. Regardless of the method by which they are formed, however, the process must be economical and the resultant films must exhibit the following characteristics: Good thickness uniformity, high purity and density, controlled composition stoichiometries, high degree of structural perfection, good electrical properties, excellent adhesion and good step coverage.

Favoured by its high refractive index, low optical absorption and high transmittance over a broad-spectrum range, Ta_2O_5 has been considered as an important candidate for the optical film material [25].

4. Deposition Techniques

Chemical vapor deposition (CVD)

CVD is defined as the formation of a non-volatile solid film on a substrate by the reaction of vapor phase chemicals (reactants) that contain the required constituents. The reaction gases are introduced into a reaction chamber and are decomposed and reacted at a heated surface to form the film. Advantages- high purity deposits can be achieved, a great variety of chemical compositions can be deposited, some films cannot be deposited with adequate film properties by any other method and good economy and process control are possible for many films [18].

Sputtering

The sputtering systems used for depositing oxides can be divided into r.f. magnetron sputtering and ion beam sputtering (IBD). In the ion

beam sputtering system, one or several Kaufman type ion guns are used to generate a broad inert gas ion beam with the accelerating voltage between 100±1500 eV. As the ion beam impinges on the target surface, the oxide materials are sputtered to deposit on a heated substrate. It has been shown that IBD can be used for growing high quality oxide thin film like PLZT and $KNbO_3$ for optical applications[18].

Pulse laser deposition

The samples grown by PLD method are highly crystalline in nature. PLD offers a variety of tunable parameters such as laser energy, background gas pressure, substrate temperature, deposition time etc. These parameters can be controlled, and thereby the growth and the properties of the resultant nanostructure samples can also be controlled [1].

Sol Gel Method

The solgel process is very versatile for preparing thin. With the solgel process, large-scale oxide can be prepared with tailored refractive indices, high dielectric constants or high ionic conductivities at lower cost compared to conventional evaporation processes. Also, the solgel process does not need expensive fabrication equipment to coat large areas and irregular substrate geometries [11].

Among all these techniques, sol-gel method has some advantages because of low pro duction costs, high chemical purity and control over the index of refraction. Large-scale oxide films can be prepared with tailored refractive indices, high dielectric constants or high ionic conductivities at lower cost compared to conventional evaporation processes. One of the most important advantages of the Sol-gel method is that, it includes an appropriate refractive index, which provides high-efficiency anti- reflection [4].

Sol-gel process, a very versatile process for making metal oxides that involves: Dissolving one or more metal organic compounds in an organic solvent, gelling the resulting solution, converting the gelled product, usually by drying and/or heat, to an oxide [13]. Although the sol-gel film has higher laser damage resistance than that of PVD film, their weakness in high temperature resistance is also apparent [25]. Summary for sol gel- Less complicated process, gel like spongy films good for high LIDT as heat dissipation is more.

Additives

There are many factors which influence the properties of the film, such as the precursor, additives and annealing temperature. There are many

types of additives, including acetylacetone (ACAC), diethanolamine (DEA), polyethylene glycol (PEG) and poly vinylpyrrolidone (PVP). These additives are capable of stabilizing nanoparticles in the sol and thus optimizing the three-dimensional network structure of the prepared film [28].

In the present study, we have used dual additives e.g. DEA and ACAC. These additives contain hydroxyl and C=O groups, respectively, both exert chelating effects. The coordination bonds can be formed between O atoms in the afore mentioned groups and Ta atoms. In other words, DEA and ACAC can bind Ta_2O_5 nanoparticles that, to some extent, provides coating effect on the particle surface. The long-chain molecular structure of PEG can suppress the mutual approach and adjacent nanoparticle agglomeration in the sol [28]. This increases the stability of the sol.

Chapter 3

Experimental Setup

Sol Gel

Defining a few terms:

- Colloid: A suspension in which the dispersed phase is so small that the gravitational forces are negligible and interactions are dominated by short range forces.
- Sol: A colloid suspension of solid particles in a liquid
- Hydrolysis: Metal alkoxide (M-OR) reacts with water to form metal hydroxide.
- Condensation: Two metal hydroxides (M-OH and HO-M) combine to give metal oxide species.
- Gel: A sponge like, 3-D solid network whose pores are filled with another substance, usually original solvent of the sol. The resultant wet gels are therefore called aquagel, hydrodel or alcogel [14].

Preparation of sol-

$M(OR)_n + nH_2O \rightarrow M(OH)_n + nROH$ (hydrolysis)
$M(OH)_n \rightarrow MO_{n/2} + (n/2)\ H_2O$ (condensation)
$M(OR)_n + (n/2)\ H_2O \rightarrow MO_{n/2} + nROH$ (overall)

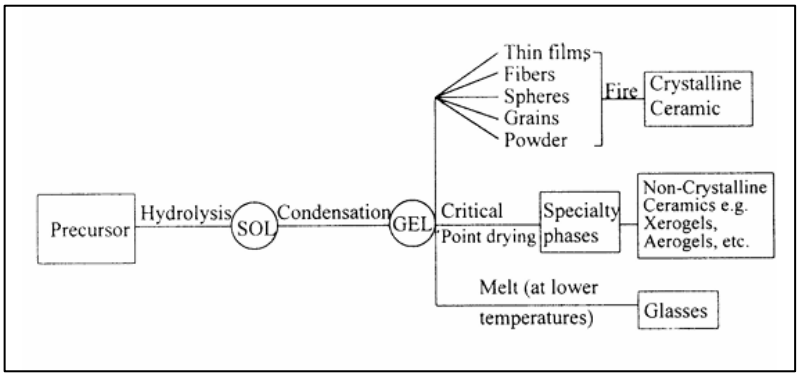

Fig.2- A flow chart describing the sol-gel process.

The factors affecting deposition during dip coating are retrieval speed, dip time etc.

Preparation of sol

For the preparation of Ta_2O_5 sol, two separate solutions were prepared. Solution 1 was prepared by mixing the precursor- tantalum ethoxide [Ta $(OC_2H_5)_5$] in 30 ml of ethanol. Further glacial acetic acid (5ml) was added for improving the viscosity as well as to promote the formation of the sol gel state. This solution was stirred for 30 minutes. Solution 2 was prepared by mixing 25ml ethanol with 5ml ethylene glycol. One or two drops were added to this solution and the solution was stirred for 30 minutes at the same time as solution 1. After the solutions were formed, solution B was slowly poured, drop by drop into solution A. This mixture was stirred for further one hour [4].

For some of the samples, before stirring for an hour, two additives were further added into this solution; acetyl acetone and diethanol amine [28]. The substrates used were fused silica and bare silicon. The films were deposited through the process of spin coating and dip coating.

Dip Coating-

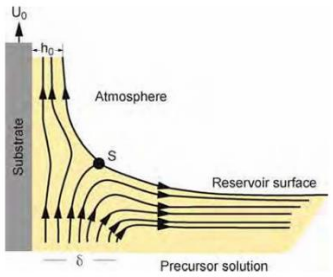

Fig.3 A dip coating unit used in the deposition. Fig. 4-Film deposition mechanism in dip coating.

In dip coating method, the sol is put into a container such as a beaker. The substrate fused silica is wound by a clean nichrome wire. The substrate is also cleaned using isopropyl alcohol. After cleaning, the substrate is hung through the wire in the dip coater. The dip coater consists of a computer software that lets the user customize a program by taking the retrieval speed, dipping speed, dipping time and other such parameters. After providing these inputs, the substrate travels downward, inside the container containing the sol at a constant speed. After dipping, the sample stays in the liquid for a designated time and then pulled out of the sol again at a constant speed. After this process, the sample is automatically taken inside an infrared heater, where it is kept for 20 minutes. This ensures proper adhesion of the film. After heating, the sample is taken out of the heater and the process is completed.

The coating process for the current project consists of the substrate to be coated with Ta_2O_5 first and then coating with SiO_2. This is done to ensure that the incident radiation should no experience a large change in refractive index but rather a gradual change- Refractive index of air-1,refractive index of SiO_2-1.45, refractive index of Ta_2O_5- 1.7, refractive index of fused silica: 1.55. Variations observed with change in retrieval speed and dip time are shown in the observations section

Spin Coating-

When a solution of a material and solvent is spun at high speeds with a spin coater, the combination of centripetal force and surface tension helps achieve a uniform coating. Once any excess solvent evaporates, spin coating produces a thin film that can range from a few nanometers to several microns in thickness.

Spin coating can be carried out in two ways- static and dynamic. The former involves dropping the solution on the substrate follwed by spinning, the latter involves dropping the sol whilst the substrate is already spinning. A dynamic dispense is preferred for its controlled process. It minimizes solvent evaporation before spinning starts, making ramp speed and dispense time less critical, provided the substrate reaches the desired RPM. Additionally, dynamic dispense typically uses less ink, although this can vary with surface wetting properties.

Details regarding the speeds and dip time for both the coaters are given in the observation section.

Chapter 4

Characterization techniques

- **UV VIS Spectroscopy to determine the nature of bandgap and estimation of bandgap**

UV VIS Spectroscopy to determine the nature of bandgap and estimation of bandgap. Direct bandgap semiconductor- maximum energy of the valence band occurs at the same value of momentum to the minimum in conduction band energy. Indirect bandgap semiconductor- maximum energy of the valence band occurs at the same value of momentum to the minimum in conduction band energy.

Beer Lambert law- $I_t=I_o\ e^{-\alpha d}$

α= absorption coefficient

d = thickness of the sample

I_t, I_o= transmitted, incident light

α (cm^-1) = 2.303A/d, A=log (I_o/I_t) = 2.303 log(1/T)

Direct band gap materials also exhibit sharp rise in absorption above the E_g in the plot of energy of light source of UV VIS setup vs absorption coefficient. Direct bandgap materials show high absorption and sharp rise in α^2 vs E.

For direct bandgap materials- $\alpha = C[hv-E_g]^{0.5}$

For indirect bandgap materials- $\alpha = C\ [hv-Eg\ -/+\ Ep]^2$

Other electronic transitions such as transition between band and impurity level manifest as shoulder in absorption data.

VW Absolute Specular Reflectance Accessory for Cary 5000

The Cary 5000 UV-Vis Spectrometer is a high-performance analytical instrument manufactured by Agilent Technologies. It is designed for a wide range of applications in various fields, including materials science, pharmaceutical research, and environmental analysis.

Working Principle:
The Cary 5000 UV-Vis Spectrometer operates on the principle of ultraviolet-visible (UV-Vis) spectroscopy. It measures the absorption or transmission of light by a sample over a specific wavelength range,

typically from 175 nm to 3300 nm, covering the ultraviolet, visible, and near-infrared regions of the electromagnetic spectrum.

The main components of the Cary 5000 UV-Vis Spectrometer are:

1. Light Source: The instrument uses a dual-lamp system, which includes a deuterium lamp for the UV region and a tungsten-halogen lamp for the visible and near-infrared regions.
2. Monochromator: The monochromator is responsible for selecting a specific wavelength of light from the broad spectrum emitted by the light sources. It uses a diffraction grating to disperse the light and select the desired wavelength.
3. Sample Compartment: The sample compartment is where the sample to be analyzed is placed. It can accommodate various sample types, such as liquids, solids, or powders, in different sample holders or cuvettes.
4. Detector: The detector, typically a photomultiplier tube or a solid-state detector, measures the intensity of the light that passes through the sample. The difference in intensity between the incident light and the transmitted light is used to calculate the absorption or transmission spectra of the sample.

Configuration:
The Cary 5000 UV-Vis Spectrometer offers a variety of configuration options to suit different analytical requirements:

1. Wavelength Range: The instrument can cover a wide wavelength range, from 175 nm to 3300 nm, allowing for the analysis of a broad range of samples.
2. Optical Configurations: The Cary 5000 can be configured with different optical layouts, such as double-beam or single-beam, depending on the specific application and the required level of sensitivity and accuracy.
3. Sample Accessories: The instrument can be equipped with a range of sample accessories, including liquid sample holders, solid sample holders, temperature-controlled sample compartments, and integrating spheres for diffuse reflectance measurements.
4. Software: The Cary 5000 is accompanied by Agilent's proprietary software, which provides advanced data analysis and reporting capabilities, as well as the ability to control the instrument and automate various measurement procedures.

Ellipsometry

Ellipsometry measures a change in polarization as light reflects or transmits from a material structure. The polarization change is represented as an amplitude ratio, Ψ, and the phase difference, Δ. The measured response depends on optical properties and thickness of individual materials.

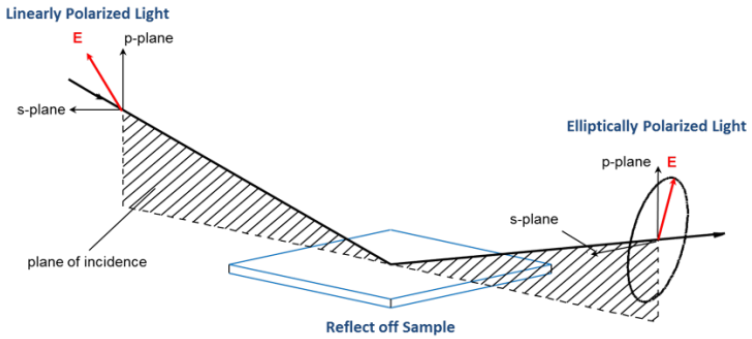

Fig. 5. Working principle of ellipsometry

The electric field of a wave is always orthogonal to the propagation direction. Therefore, a wave traveling along the z-direction can be described by its x- and y- components.
When the light has completely random orientation and phase, it is considered unpolarized. For ellipsometry, however, we are interested in the kind of electric field that follows a specific path and traces out a distinct shape at any point. This is known as polarized light. If the orthogonal waves are 90° out-of-phase and equal in amplitude, the resultant light is circularly polarized. The most common polarization is "elliptical", one that combines orthogonal waves of arbitrary amplitude and phase.
Ellipsometry is primarily interested in how p- and s- components change upon reflection or transmission in relation to each other. In this manner, the reference beam is part of the experiment.

The incident light is linear with both p- and s- components. The reflected light has undergone amplitude and phase changes for both p- and s- polarized light, and ellipsometry measures their changes.
The primary tools for collecting ellipsometry data all include the following: light source, polarization generator, sample, polarization analyzer, and detector. The polarization generator and analyzer are constructed of optical components that manipulate the polarization: polarizers, compensators, and phase modulators.

Laser Induced Damage Threshold

A laser beam is directed towards optics at different locations and optics is observed carefully for any damage under microscope. This LIDT test setup consists of a pulsed Nd: YAG laser, which can give up to 0.5 J per pulse with 1-10 Hz repetition rate at 1064 nm and a typical pulse width of 5-6 ns (FWHM). Damage morphology is recorded with Nomarski DIC microscope.

Photothermal absorption

When a laser hits any optical element, the incident radiation causes heat generation due to the intense power of the laser. This heat is absorbed by the thin film or the optical element. The absorption coefficient is calculated by this technique.

Two lasers are present- a pump laser and a probe laser. The pump laser causes the heating; the pump laser creates the interference effects that can be studied.Absorption is tested at the wavelength of a pump laser. Probe beam senses the heating effect of absorbed pump. Periodic heating provided by the chopped pump results in periodic perturbation of the probe beam shape. The photothermal signal comes as a small modulation of a relatively big photodetector current. The average current, the DC signal, and the small modulation of it at the chopping frequency, AC signal, define the modulation depth AC/DC which is proportional to absorption [29]. The phase distortion relies on the index of refraction distortion and/or thermal expansion of the tested material. The 0.1 ppm estimate is valid for most glasses and many crystals.

Calculating flatness- Newton's ring and Fizeau interferometer

Fig.6 An image of the pattern seen under a light source during the Newton's ring experiment

Newton's ring method:

A sodium lamp of wavelength 532nm is used as a light source. A few glass pieces known as masters are used for which the flatness is known

The following formula is used-

$$\boldsymbol{E = \frac{\Delta d \times \lambda}{D \times 2}}$$

Δd is the fringe thickness, D is the diameter of the sample, λis the wavelength of the sodium lamp, the thickness is given in terms of λ

Fizeau interferometer (FI)

Fizeau interferometer is one of the most important optical metrology instruments at optics development facilities and laboratories for non-contact surface measurements of polished optical surfaces. A polarization phase shifting Fizeau interferometer has been developed for quantitative evaluation of surface flatness and 3-D surface form of polished optical surfaces.

FI is a two-beam interferometer, where the interference is formed between the beams reflected, from reference flat surface and test surface. The shape of the interference fringes qualitatively represents the shape of the test surface.Phase shifting interferometry is most useful and accurate method for quantitative measurement of phase information of the test optics. The phase information can be converted to height variations and a 2-D surface form of the test optics can be obtained. The displacement of the Fizeau fringes from the ideal straight, parallel pattern can be measured and used to calculate the surface flatness.

The formula to calculate the surface flatness is:

Surface flatness = (N * λ) / 2

N is the number of Fizeau fringes across the test surface, λ is the wavelength of the light source

Chapter 5

Observations and Results

Sample details

Spin coating:

Speed (RPM)	Sol	Substrate	Acceleration (μ/s^2)	Spin time (s)
3500	Ta_2O_5	Fused Silica	1000	30
3500	Ta_2O_5	Bare Silicon	1000	30

Dip coating

Sample	Thickness (nm)	Refractive Index	Wavelength (nm)	%T	Bandgap (eV)
SiO_2	135	1.44	550	90.3	
Ta_2O_5	102	1.71	550.5	93.2	4.2

1. Effect of speed in spin coating

In general, the thickness of a spin coated film is proportional to the inverse of the square root of spin speed as in the below equation where ω is angular velocity/spin speed and h_f is final film thickness.

$$h_f \propto \frac{1}{\sqrt{\omega}}$$

This means that a film that is spun at four times the speed will be half as thick. The exact thickness of a film will depend upon the material concentration and solvent evaporation rate, which in turn depends upon the solvent viscosity, vapor pressure, temperature and local humidity [27].

2. Effect of retrieval speed in dip coating

In principle a competition between various forces in the film deposition region governs the film thickness and the position of the stream line. When the liquid viscosity η and withdrawal speed U_0 are high enough to lower the curvature of the gravitational meniscus, the deposited film thickness h0 is that which balances the viscous drag (ηU0) and gravity force (ρg) according to: $h_o = c_1\sqrt{\frac{nU_o}{\rho g}}$

where ρ is the liquid density, g is the acceleration of gravity and the constant c_1 is about 0.8 for Newtonian liquids. When the substrate speed (typical range of ~1–10 mm/s) and liquid

viscosity η are low, as is often the case for sol-gel film deposition, this balance (Eq. 10.1) is modulated by the ratio of viscous drag to liquid-vapor surface tension γ LV, according to the relationship derived by Landau and Levich for a Newtonian and non-evaporating fluid:

$$h_0 = 0.94 \frac{(nU_o)^{2/3}}{\gamma_{LV}^{1/6}(\rho g)^{1/2}}$$

In case of very low withdrawal speeds, i.e. in the capillarity regime, the solvent evaporation becomes faster than the movement of the drying line leading to a continuous feeding of the upper part of the meniscus by the precursor solution through capillary rise .By assuming that the evaporation rate E is constant and applying the mass conservation law the following relation for the final film thickness h_f (i.e. after stabilization by thermal treatment) could be derived for the capillarity regime :

$$h_f = \frac{c_i m_i E}{\alpha_i \rho_i U_o L}$$

3. Effect of dip duration in dip coating

The longer the sample is kept inside the solution, the better is the adhesion of the solution on the substrate. The longer a substrate is kept inside the solution, the thicker is the film.

4. Effect of additives

With no additives, the particles agglomerate rapidly during hydrolysis and polycondensation reactions, which results in large Ta_2O_5 clusters formation. The additives exert a coating effect over the nanoparticle surface leading to improvement in sol stability. The −OH and C=O groups contained in the additives exert chelation effects resulting in an appropriate three-dimensional network structure with less internal defects leading to superior optical properties. Sol stability is expected to lead to higher LIDT.

5. Effect of number of layers/ coatings

The number of coatings increases the thickness of the film in total, although the inherent properties show no significant difference, i.e, same results can be obtained with thinner films. Multiple layers are useful in case we want different transmissions at different wavelengths.

Ta_2O_5 thin film	Dip time (s)	Retrieval speed (µm/s)	Film thickness of Ta_2O_5 (nm)	Inference	LIDT (J/cm^2)
Ta_2O_5-P	60	2000	90	Good surface coverage	13.8
Ta_2O_5-Ad	60	2000	100	Moderate surface coverage	15.4
Ta_2O_5-Ad	120	2000	113	Surface coverage increases	
Ta_2O_5-Ad	180	2000	133	Surface coverage increases significantly	
Ta_2O_5-Ad	180	3000	164	Good surface coverage	

Table-3. Ta_2O_5 thin film properties with varying dip coating deposition parameters.

First, the film morphology, thickness and optical properties of Ta_2O_5-Ad single layer were characterized and the results are shown in Table-3. Fig. 7 shows that increase in dip duration not only improves the surface coverage of the film [Fig. 7] but also increases the film thickness as shown in Table-3. Maximum transmission value remained unchanged. With increase in retrieval speed from 2000 µm/s to 3000 µm/s the film thickness increases from 133 to 164 nm. RMS roughness of the Ta_2O_5-Ad film was calculated to be 2.6 Å as shown in Fig.7. The refractive index values were derived from fitting the transmission spectrum of the respective film through Optilayer software. The same was confirmed from spectroscopic ellipsometry measurement also.

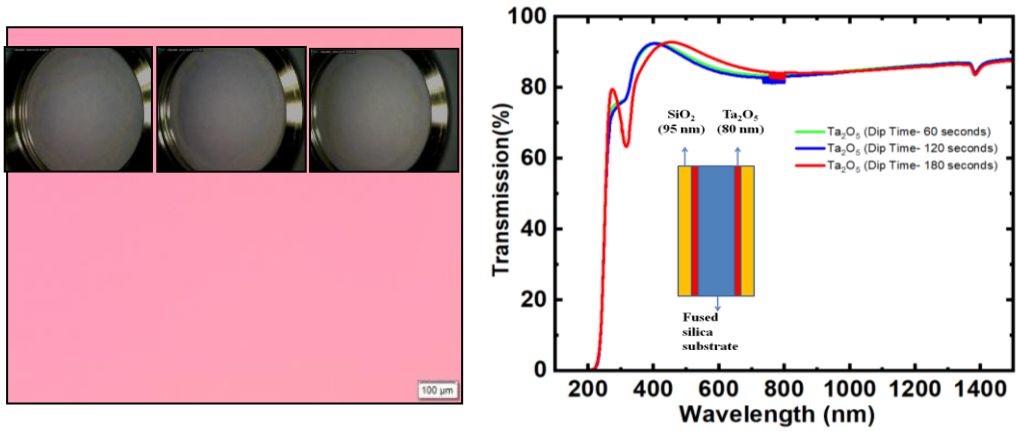

Fig.7- Optical image of a representative Ta_2O_5 coating with varying dip time.

Fig. 8 - Comparison of transmission spectra of Ta_2O_5 films with varying dip time.

For AR coating a Ta_2O_5/SiO_2 bilayer structure was designed using Optilayer software. Film morphology was imaged using a multimode scanning probe microscope (NT-MDT, SOLVER-PRO). Transmission was measured using Cary 5000 using V-W configuration and film thickness was measured through SOPRA GES-5 ellipsometer. Laser induced damage threshold (LIDT) experiment was carried out using a 1064 nm Q-switched pulsed Nd:YAG laser at a pulse length of 6–7 ns and repetition rate of 1 Hz. The laser was focused to form a circular Gaussian beam and the spot size was 0.28 mm.

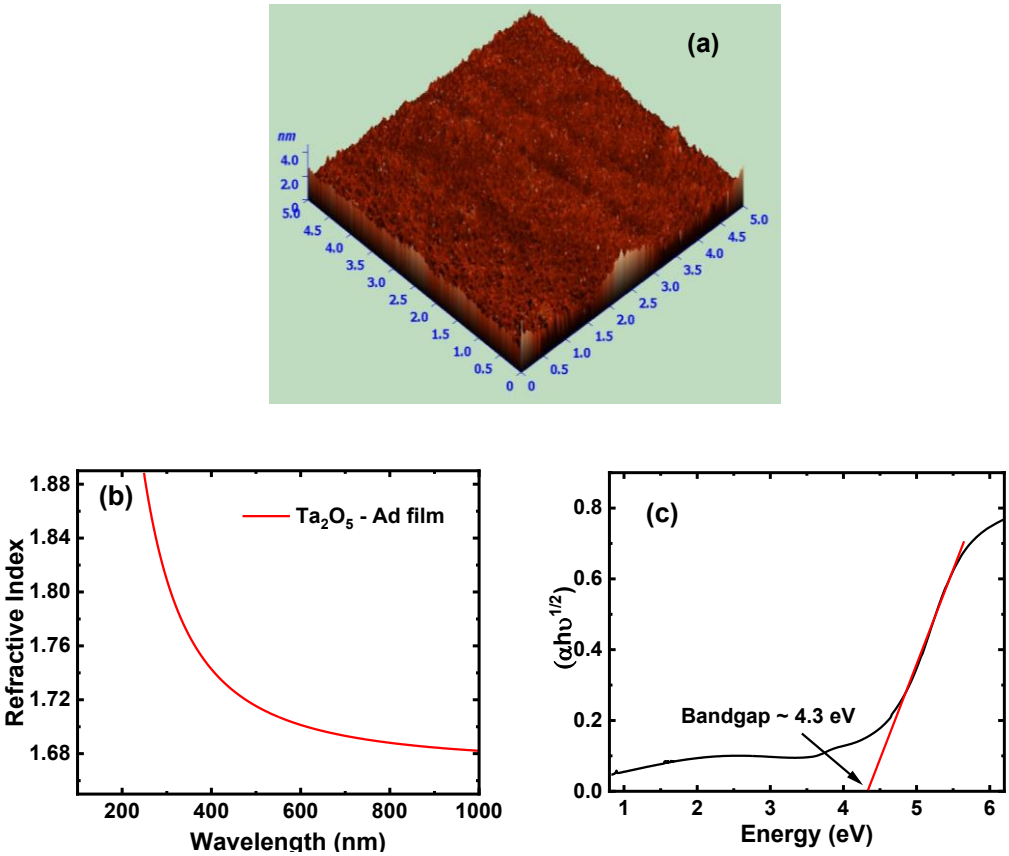

Fig.9. (a) 2D AFM image of Ta_2O_5-Ad. (b) Wavelength dependent refractive index of Ta_2O_5-Ad film. (c) Bandgap estimation of Ta_2O_5 from transmission spectrum.

The increase in film thickness with increase in dip time is also revealed in the transmission spectra of the corresponding films as shown in Fig.8. Maximum transmission value remains unchanged. With increase

in retrieval speed from 2000 μm/s to 3000 μm/s the film thickness increases from 133 to 164 nm. RMS roughness of the Ta_2O_5-Ad film was calculated to be 2.6 Å [Fig.9(a)], which is same as Ta_2O_5-P film. The refractive index values were derived from fitting the transmission spectrum of the respective film through Optilayer software. The same was confirmed from spectroscopic ellipsometry measurement also. The absorption has been derived from the transmission curves and the bandgaps are calculated from the $(\alpha h\nu)^{1/2}$ vs. $h\nu$ plot as shown in Fig. 9(c). The refractive index and direct bandgap of Ta_2O_5-Ad film was found to be 1.71 and 4.3 eV, respectively, as shown in Fig.9(b) and 9(c). Whereas, the same for Ta_2O_5-P film was 1.67 and 4.46 eV, respectively. We can therefore infer that additives play a significant role in modifying the optical properties of the Ta_2O_5 thin film without affecting its morphology.

Next, we will discuss how these change in properties is manifested in the optical device performance. Ta_2O_5 /SiO_2 AR coatings were deposited on both sides of FS substrates using both Ta_2O_5-P as well as Ta_2O_5-Ad through dip coating method. A schematic deposition diagram is shown in the inset of Fig.6.

Results on AR coating:

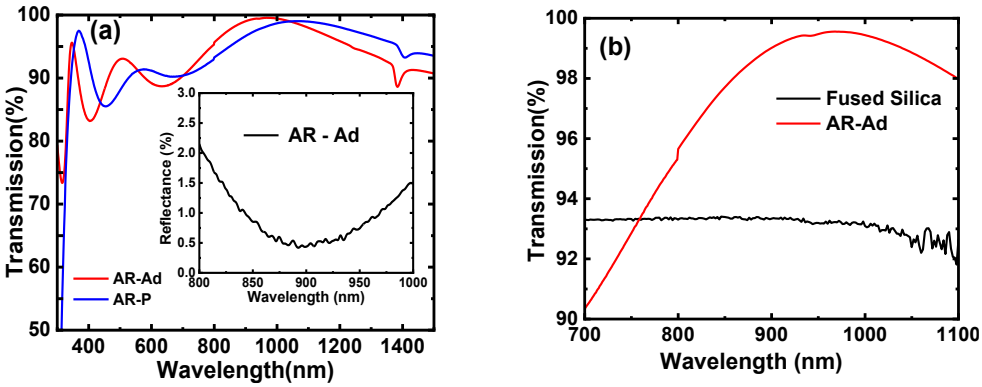

Fig.10. (a) Transmission spectra of AR-Ad vs. AR-P. Inset: Reflectivity spectrum of AR-Ad. (b) Transmission spectra of AR-Ad and Fused silica.

AR-Ad exhibited 99.6% maximum transmission at ~ 968 nm with transmission of over 99% in the range of 900-1040 nm. The maximum

transmission as well as the band width (%T > 99%) of the AR-Ad coating is clearly increased compared to AR-P as furnished in Table-4 and Fig. 10(a). The enhancement in transmission as well as FWHM may be attributed to the higher refractive index value of the Ta_2O_5-Ad compared to Ta_2O_5-P. The reflectivity spectrum of the AR-Ad is shown in the inset of Fig. 8(a).

With no additives, the particles agglomerate rapidly during hydrolysis and polycondensation reactions, which results in large Ta_2O_5 clusters formation. The additives exert a coating effect over the nanoparticle surface leading to improvement in sol stability. The −OH and C=O groups contained in the additives exert chelation effects resulting in an appropriate three-dimensional network structure with less internal defects leading to higher LIDT.

Ta_2O_5 /SiO_2 AR coating	Film thickness Ta_2O_5 / SiO_2 (nm)	Refractive index Ta_2O_5/SiO_2	Transmission (%)	Bandwidth %T > 99% (nm)	LIDT (J/cm^2)
AR-P	177/176	1.67 /1.45	99.1 % @ 1053 nm	36	20.1
AR-Ad	150/160	1.71 /1.45	99.6 % @ 968 nm	140	19.7

Table-4. Comparison between various optical parameters of the Ta_2O_5 /SiO_2 AR coatings, with and without additives.

Photothermal absorption study:

Absorption coefficient was obtained by photo-thermal common path interferometer (PCI) technique (M/s Stanford Photothermal).

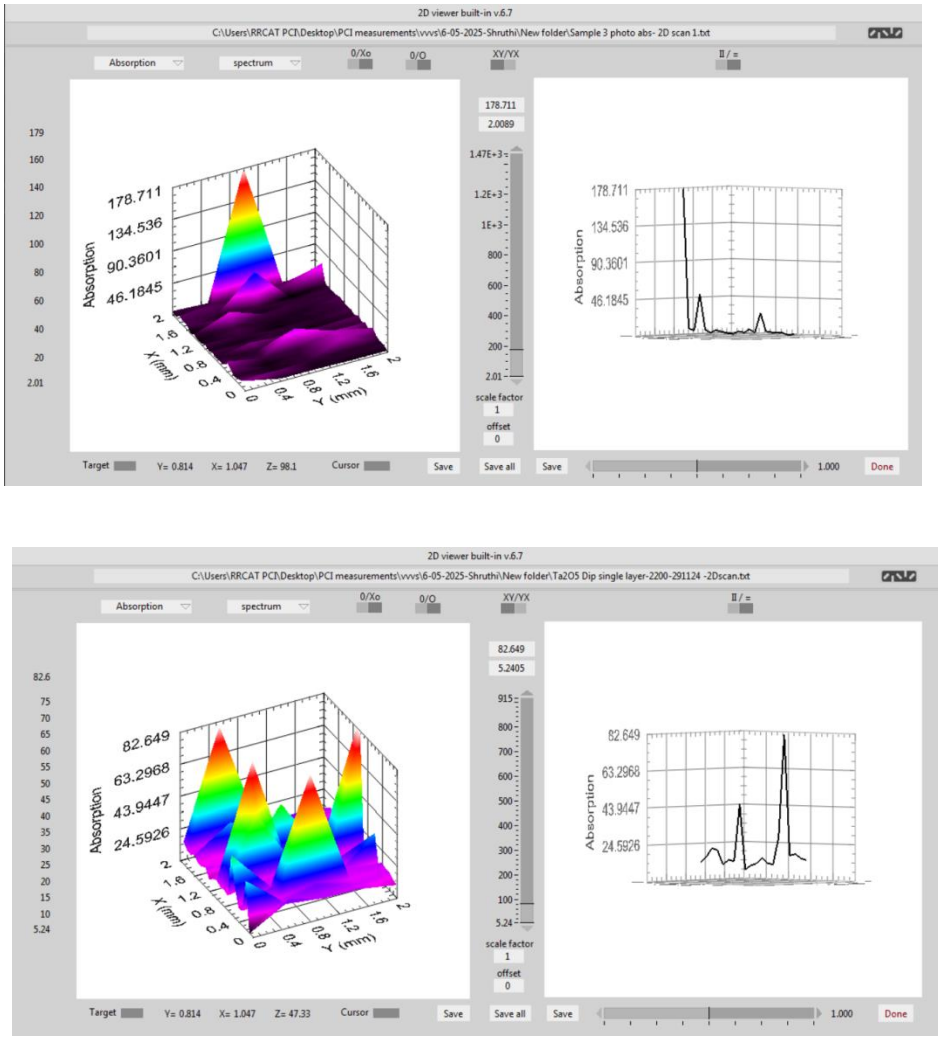

Fig.11- Photothermal absorption plots of absolute absorption coefficient at 532nm wavelength. (a) Ta_2O_5 single layer. (b) AR

The photothermal absorption was measured to be ~50 ppm for the Ta2O5 single layer thin films. The same for the AR coatings were measured to be ~60 ppm. The individual scattered spikes in absorption may be attributed to dust particles present on the films as the films were preserved in normal atmosphere for long time.

Characterization of the surface figure

The stress introduced in the test optics was evaluated using a polarization phase-shifting Fizeau interferometer. The interferometer generates five 90° phase-shifted interferograms, and the surface parameters were determined by evaluating the phase map obtained from the phase wrapping and unwrapping of the interferograms' intensity data. Fig.12 (a), and (d) exhibit the representative phase-shifted interferograms; Fig.12 (b) and (e) represent 2D phase maps; and Fig. 12 (c) and (f) represent the height profiles of the respective sample surfaces. The bare FS substrate surface exhibits concave curvature with surface figure λ/10 [not shown in figure]. The surface figure value changes in the coated samples due to stress development in the films. Stress generation in thin films deposited through various techniques, sol-gel process in particular. Generated stress increases with reduction in film thickness. In sol-gel spin coated thin film, magnitude of stress depends on deposition conditions such as viscosity of the sols, spin speed, heating and cooling rate etc. During drying at low temperature @ 90ºC as in the present case, evaporation of solvents and solvent/polymeric network interactions led to constrained shrinkage of the films giving rise to compressive stress as observed in the following figures [Fig.12]. The surface figure of the Ta_2O_5 single layer as well as AR coating was measured to be λ/4 [PV (λ) ~ 0.2] [9].

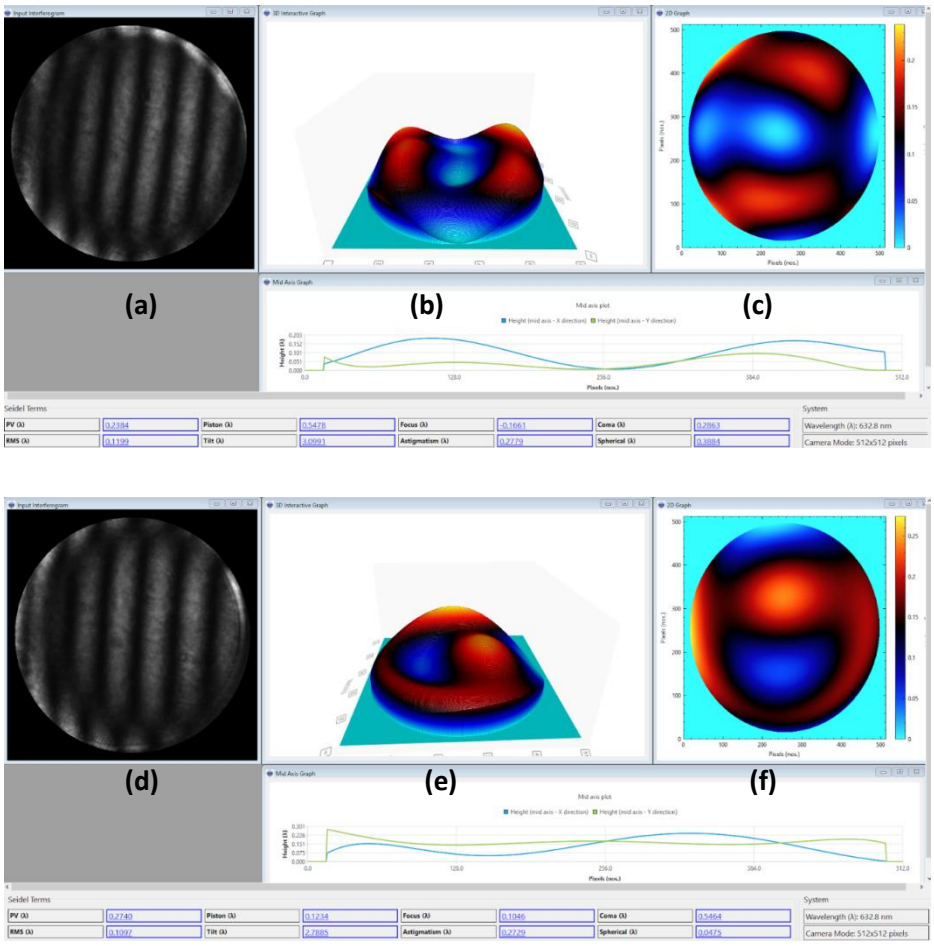

Fig.12. (a,d) Representative interferograms. (b, e) 2D phase maps. (c,f) Height profiles along X- and Y- direction. Top to bottom: Single layer Ta_2O_5 single layer thin film and AR coating.

LIDT measurement

Next for laser induced damage threshold, a functional analysis was performed for the single layer Ta_2O_5 thin film as well as AR coatings. The LIDT value for the Ta_2O_5-Ad single layer improved to 15.4 J/cm^2 (50% damage probability) as compared to 13.8 J/cm^2 (100%) of Ta_2O_5-P . Damage profile for Ta_2O_5-Ad film is shown in Fig.11 . Both AR-P and AR-Ad exhibited LIDT value ~20 J/cm^2. This might be attributed to the LIDT property of the top SiO_2 layer in the AR coatings which

remained same for both the cases. Further study of improvement in the top SiO_2 layer is under the scope of future study.

Fig.13- Laser damage profile for additive assisted deposited Ta_2O_5 film.

Chapter 6

Conclusions and Scope for Future Work

Effects of addition of acetyl acetone and diethylamine additive is studied. Variation of dip duration, retrieval speed in the thin film properties is analyzed.35

The refractive index and energy bandgap were found to be 1.71 and 4.3 eV, respectively for the additive assisted Ta_2O_5 thin film.

Additive played a significant role in reducing reflectivity of the AR coating and increasing the bandwidth. Additives also facilitate increase in LIDT of the thin film.

Ta_2O_5/SiO_2 AR coating with 99.6% transmission and 140 nm bandwidth along with an LIDT value of ~20 J/cm^2 was obtained through dip coating.

Role of additives: With no additives, the particles agglomerate rapidly during hydrolysis and polycondensation reactions, which results in large Ta2O5 clusters formation.

The additives exert a coating effect over the nanoparticle surface leading to improvement in sol stability. The −OH and C=O groups contained in the additives exert chelation effects resulting in an appropriate three-dimensional network structure with less internal defects leading to superior optical properties. Sol stability is expected to lead to higher LIDT.

REFERENCES

[1] Synthesis and study of crystallographically oriented Zinc Oxide (ZnO) nanostructures- PhD thesis - Ankit Soni

[2] Effects of substrates on the crystalline growth and UV photosensitivity of glancing angle deposited porous ZnO nanostructures-Ankit Soni, Komal Mulchandani, K. R. Mavani

[3] UV activated visible-blind Ga:ZnO photodetectors using the GLAD technique: A comparative study under different gas atmospheres and temperatures-Ankit Soni, Komal Mulchandani, K. R. Mavani

[4] Sol-gel prepared amorphous Ta2O5 thin film for application in high LIDT antireflection coating and UV photodetection-Suparna Pal, Rajiv Kamparatha, V.V.V. Subrahmanyama, Neha Sharma et al.

[5] Ultrafast self-powered visible blind UV photodetectors based on MgZnO vertical Schottky junction in crossbar geometry - Amit K. Das et al.

[6] Solar-blind UV detectors based on wideband gap semiconductors-Udo Sch¨uhleI and Jean-Franc¸ois Hochedez

[7] Controlling porosity and ultraviolet photoresponse of crystallographically oriented ZnO nanostructures grown by pulsed laser deposition-Ankit Soni, K.R. Mavani

[8] The Use of UV-visible Spectroscopy to Measure the Band Gap of a Semiconductor -Zhebo Chen and Thomas F. Jaramillo

[9] PMMA as an Additive for Nanostructured TiO2 Thin Films for Heterojunction Visible-Blind Photodetectors- Suparna Pal, Rajiv Kamparatha, V.V.V. Subrahmanyama, Neha Sharma et al.

[10] Anti reflecting coating from Ta2O5 and SiO2nmultilayer films- K. KOC,F.Z. TEPEHAN, G.G. TEPEHAN

[11] Optical properties of sol}gel dip-coated Ta 2O5 films for electrochromic applications Ferhad E. Ghodsi et al

[12] Introduction to Optics - Third Edition -FRANK L. PEDROTTI

[13] Optical coatings by Sol Gel processes-Energy and Technology review Lawrence Livermore National Laboratory October 1985

[14] Review on sol gel derived coatings- S.M. Attia et al.

[15] Laser Facet Coating – Mtech report- Ruby Jain (SGSITS and RRCAT, Indore)

[16] Optical properties of sol}gel dip-coated Ta2O5 films for electrochromic applications Fatma Z. Tepehan et al.

[17] Heat treatment e!ects on the optical properties of Sol gel Ta2O5 thin films Farhad E. Ghodsi, Fatma Z. Tepehan\

[18] Preparation and properties of tantalum pentoxide(Ta2O5) thin ®lms for ultra large scale integrated circuits (ULSIs) application -A reviewS. EZHILVALAVAN, T. Y. TSENG

[19] Optical properties of Ta205 thin films deposited using the spin coating process Farhad E. Ghodsi, Fatma Z. Tepehan, Galip G. Tepehan

[20] Determination of optical properties of amorphous Ta205 films deposited by spin- and dip-coating methods Fatma Z. Tepehan , Farhad E. Ghodsi , Nilgun Ozer , Galip G. Tepehan

[21] Gas pressures influence on the optical and mechanical properties of Ta2O5 films produced by reactive low voltage ion plating (RLVIP) G.N. Strauss, W. Lechnera , H.K. Pulker

[22] Optical properties of amorphous Ta2O5 thin films deposited by RF magnetron sputtering Xinyi Chen , Rui Bai , Meidong Huang

[23] High temperature annealing effect on structure, optical property and laser-induced damage threshold of Ta2O5 films Cheng Xu, Qiling Xiao,Jianyong Ma, Yunxia Jin, Jianda Shao , Zhengxiu Fan

[24] Effects of deposition parameters on laser-induced damage threshold of Ta2O5 filmsCheng Xu , Yinghuai Qiang , Yabo Zhu , Jianda Shao ,ZhengxiuFan , Jinhong Han

[25] In-situ high temperature laser-induced damage of sol-gel Ta2O5 films with different dual additives Pu Zhang (ConceptualizationMethodologyWriting), Di Lin (Data curationWriting – original draft), Yongqiao Zhua, Wenzhe Caia, Dawei Lib, Cheng Xu

[26] Laser-induced damage of Ta2O5 films obtained from $TaCl_5$ precursor

[27] Dip Coating C. Jeffrey Brinker

[28] In-situ high temperature laser-induced damage of solgel Ta2O5 films withdifferent dual additives-Pu Zhang et al